From in vitro evaluation to human postmortem pre-validation of a radiopaque and resorbable internal biliary stent for liver transplantation applications

Edouard Girard, Grégory Chagnon, Alexis Broisat, Stéphane Dejean, Audrey Soubies, Hugo Gil, Tahmer Sharkawi, François Boucher, Gael S Roth, Bertrand Trilling, et al.

From in vitro evaluation to human post-mortem pre-validation of a radiopaque and resorbable internal biliary stent for liver transplantation applications

Edouard GIRARD[1,2,3,*], Grégory CHAGNON[1], Alexis BROISAT[4,5], Stéphane DEJEAN[6] Audrey SOUBIES[4,5], Hugo GIL[7], Tahmer SHARKAWI[8], François BOUCHER[1,5], Gaël S ROTH[9,10], Bertrand TRILLING[1,2,3], Benjamin NOTTELET[6,*]

[1] Univ. Grenoble Alpes, CNRS, CHU Grenoble Alpes, Grenoble INP, TIMC-IMAG, F-38000 Grenoble, France

[2] Département de chirurgie digestive et de l'urgence, Centre Hospitalier Grenoble-Alpes, 38000 Grenoble, France

[3] Laboratoire d'anatomie des Alpes françaises (LADAF), UFR de médecine de Grenoble, Université de Grenoble-Alpes, F-38700 Grenoble, France.

[4] INSERM, Unité 1039, F-38000 Grenoble, France

[5] Radiopharmaceutiques Biocliniques, Université Grenoble-Alpes, F-38000 Grenoble, France

[6] IBMM, Université de Montpellier, CNRS, ENSCM, Montpellier, France

[7] Département d'anatomopathologie et cytologie, Centre Hospitalier Grenoble-Alpes, 38000 Grenoble, France

[8] ICGM, Université de Montpellier, CNRS, ENSCM, Montpellier, France

[9] Institute for Advanced Biosciences, INSERM U1209/CNRS UMR 5309, Université Grenoble-Alpes, F-38700 Grenoble, France

[10] Clinique universitaire d'Hépato-gastroentérologie et Oncologie digestive, CHU Grenoble-Alpes

*** Corresponding authors:**

Dr Edouard GIRARD, Laboratoire TIMC-IMAG, Domaine de la Merci, 38706 La Tronche Cedex, France. E-mail address: edouard.girard@univ-grenoble-alpes.fr

Prof. Benjamin NOTTELET, Institut des Biomolécules Max Mousseron, UFR Pharmacie, 15 Avenue Charles Flahault, 34093 Montpellier cedex 05, France. Tel: +33 (0)411759697. E-mail address: benjamin.nottelet@umontpellier.fr

Declarations of interest: none

KEYWORDS

Liver transplantation; Internal Biliary Stenting; Absorbable Implants; Radiopaque poly(ε-caprolactone); Mechanical properties ; x-ray computed tomography scanner.

ABSTRACT

The implantation of an internal biliary stent (IBS) during liver transplantation has recently been shown to reduce biliary complications. To avoid a potentially morbid ablation procedure, we developed a resorbable and radiopaque internal biliary stent (RIBS). We studied the mechanical and radiological properties of RIBS upon in vivo implantation in rats and we evaluated RIBS implantability in human anatomical specimens.

For this purpose, a blend of PLA_{50}-PEG-PLA_{50} triblock copolymer, used as a polymer matrix, and of X-ray-visible triiodobenzoate-poly(ε-caprolactone) copolymer (PCL-TIB), as a radiopaque additive, was used to design X-ray-visible RIBS. Samples were implanted in the peritoneal cavity of rats. The radiological, chemical, and biomechanical properties were evaluated during degradation. Further histological studies were carried out to evaluate the degradation and compatibility of the RIBS. A human cadaver implantability study was also performed.

The in vivo results revealed a decline in the RIBS mechanical properties within 3 months, whereas clear and stable X-ray visualization of the RIBS was possible for up to 6 months. Histological analyses confirmed compatibility and resorption of the RIBS, with a limited inflammatory response. The RIBS could be successfully implanted in human anatomic specimens. The results reported in this study will allow the development of trackable and degradable IBS to reduce biliary complications after liver transplantation.

1. INTRODUCTION

Reconstruction of the bile duct in liver transplantation (LT) can be incorrectly considered to be the most straightforward part of what is otherwise a difficult surgical intervention. Postoperative morbidity and mortality related to biliary complications can ultimately compromise the outcomes [1–3]. Complications from bile duct anastomosis (leakage, stricture) are often considered to be the technical Achilles heel of LT. The anastomotic biliary complication rate in the literature remains high, at 10 to 50% [4]. Duct-to-duct reconstruction with T-tube insertion has been used to lower pressure in the biliary tract and decrease anastomotic complications [2,5–7]. More and more surgical teams have abandoned this technique due to the increase in specific T-tube induced complications and because secure, effective, and inexpensive outcomes can be achieved without the use of T-tubes [8–13]. The placement of an internal biliary stent (IBS) has been portrayed as a secure alternative to T-tube insertion in LT, allowing for a reduction in the morbidity of biliary anastomosis [14–17]. The absence of choledochotomy during IBS insertion is a real advantage, as choledochotomy is a source of bile leakage after a T-tube placement [5,18]. Although use of an IBS is an attractive option, a number of technical issues such as the material used (silastic, rubber) require further refinement. In particular, the main disadvantage of the materials currently used is their non-degradability, which leads to an additional surgical procedure for ablation, thereby giving rise to additional costs and potential complications.

The ideal technique could be duct-to-duct reconstruction with intraoperative insertion of a Resorbable Internal Biliary Stent (RIBS). This, unlike the silastic stent, avoids a device ablation procedure. To be usable and useful, RIBS must comply with the various specifications. RIBS must be biocompatible and generate non-toxic degradation byproducts. In order to reduce the incidence of anastomotic biliary leakage and anastomotic biliary stricture reported in the literature [19,20], a RIBS must retain its mechanical properties to calibrate and seal the

anastomosis for 8 weeks. At a practical level, it must be flexible enough to be readily implantable during LT, so as not to complicate the biliary anastomosis procedure. RIBS visualization by conventional imaging techniques during the postoperative period is also essential, in order to be able to diagnose or eliminate biliary complications related to the device (an obstruction for example). Finally, it must be fully resorbed in approximately 6 months, without inducing an excessive inflammatory response.

Degradable polymers come to mind as a way to meet these requirements. Indeed, many degradable polymers such as polyglycolide, polylactide, and their copolymers are used for the industrial manufacture of implantable medical devices such as surgical sutures, bone fixation devices, drug delivery systems, stents, and scaffolds [21–25]. Degradable stents are also being developed in clinical practice for numerous applications, including vascular applications, which reflects the high level of safety of these devices [24,26]. Several studies have been conducted since 2006 in regard to the biliary system. Xu *et al.* in 2009 investigated the degradation of a degradable poly(L-lactide-*co*-glycolide) (PLGA) stent in vitro in bile [27]. The physicochemical and mechanical characteristics were compatible with bile duct implantation, but complete degradation occurred at approximately 4-5 weeks, which is not long enough for LT. Several studies have investigated stent degradation in the bile ducts of large animals (dogs and pigs). All of these demonstrated good biocompatibility and no bile sludge stent obstruction [28–31]. As a result, in 2009, Tashiro was the first to focus on the use of these degradable devices for LT [31].

These examples highlight the fact that the kinetics of degradation and the mechanical properties are crucial data for the selection of the materials. To match both of these criteria, copolymers of aliphatic polyesters and polyether are thought to be suitable candidates as they offer a large range of mechanical properties and degradation times, while they have also been approved by regulatory agencies for various applications. Many studies have, therefore, focused on

poly(lactide)/poly(ethylene glycol) copolymers (PLA/PEG) in tissue engineering applications, ranging from vascular grafts to nerve guides and bone scaffolds [32–36]. In particular, we developed PLA-*b*-Poloxamer-*b*-PLA and PLA-*b*-Poloxamine-*b*-PLA triblock copolymers for ligament tissue engineering [37,38], and we have studied the non-linear viscoelastic behavior of PLA-*b*-PEG-*b*-PLA during their degradation to evaluate their potential for soft-tissue reconstruction [39,40].

However, a major limitation of such copolymers is their intrinsic X-rays transparency. Visualization of resorbable devices by conventional imaging means, particularly by X-rays, is essential for post-implantation monitoring. Several solutions have been proposed, in particular with the development of materials in the field of interventional radiology. A first option is the addition of radiopaque biocompatible markers on the biliary stent, as used in the treatment of benign biliary stenosis in interventional radiology [41–43]. These metallic markers, made of gold or platinum, only allow visualization of the stent position and not the stent itself, without providing information regarding the extent of the degradation. The markers may detach from the stent during the degradation. The second option is to make a radiopaque stent by the addition of an X-ray-absorbing additive such as metal powders or metal salts based on tantalum, barium, bismuth, gold, *etc.* [44–46]. For example, Lamsa *et al*. reported regarding a radiopaque stent composed of PLA_{96} with 25 wt% BaSO4 that was used to produce radiopaque bioabsorbable biliary stents [47,48]. To circumvent the problem of potential toxicity encountered with metallic additives [49], organic radiopacifiers containing heavy atoms such as bromine or iodine are also an option. However, the resulting polyester/radio-opacifier blends also suffer from leaching problems that result in the loss of imaging capabilities and potential toxicities [50]. To avoid leaching, two strategies have been described in the literature. The first one relies on covalent grafting of radiopacifiers (generally iodinated molecules) to a polymer backbone, either by using radiopaque initiators or by post-polymerization modification. In a second

approach, radiopaque monomers (generally iodinated monomers) are copolymerized to yield radiopaque copolymers. To the best of our knowledge, we were the first to describe a radiopaque polyester, namely poly(ε-caprolactone-*co*-α-iodo-ε-caprolactone) (PCL-I) containing between 10 to 25% iodized-units [51]. However, despite the X-ray radiopacity, the instability of the carbon–iodine bond prevented the use of such a copolymer for long-term visualization. Other groups have focused on the use of radiopaque initiators or chain ends to yield X-ray-visible (co)polyesters, which is a strategy that leads to a low overall content of the radiopacifier (a maximum of one initiator per chain) [52,53]. To tackle this limitation, we described the synthesis and improved stability of a radiopaque PCL-based additive for X-ray imaging, poly(ε-caprolactone-*co*-α-triiodobenzoate-ε-caprolactone) (PCL-TIB), with a higher iodine content compared to PCL-I [54]. We also showed that PCL-TIB can readily be blended with (co)polyester matrices to induce a stable X-ray opacity with as low as 2.5 wt% iodine in the blend, without significantly impacting the mechanical properties.

In the present work, our aim was to design radiopaque RIBS by taking advantage of the favorable mechanical properties of the PLA-PEG-PLA with respect to IBS application, and of the clinical imaging opportunities offered by the PCL-TIB macromolecular contrast agent. We also sought to evaluate the feasibility of implantation of RIBS in human bile ducts upon LT. More specifically, following implantation in rat peritoneum, we first compared and discuss the in vitro *vs.* the in vivo degradation and the mechanical properties of PCL-TIB/PLA-PEG-PLA over a 6-month period. We also assessed the in vivo radiological performance and the biocompatibility of this radiopaque biomaterial through computed tomography (CT) imaging and histological studies over 6 months. Finally, we evaluated the post-mortem implantability and the clinical imaging capacities of a prototype of RIBS in human cadavers.

2. MATERIALS AND METHODS

2.1. Chemicals

Poly(ε-caprolactone) (PCL, $\overline{M_n}$ = 32 000 g.mol^{-1}, Đ = 1.8), 2,3,5-triiodobenzoic acid (TIBA, 98%), thionyl chloride (97%), lithium diisopropylamide (LDA, 2 M in THF/heptane/ethylbenzene), poly(ethylene glycol) (PEG, $\overline{M_n}$ = 20 000 g.mol^{-1}), and tin(II) 2-ethylhexanoate ($Sn(Oct)_2$, 95%), were purchased from Sigma-Aldrich (St-Quentin Fallavier, France). D,L-lactide (D,L-LA) was purchased from Purac (Lyon, France). Ammonium chloride (NH_4Cl, > 99%) was obtained from Acros Organics (Noisy-le-Grand, France), technical grade magnesium sulfate ($MgSO_4$) from Carlo Erba (Val de Reuil, France), Harris's hematoxylin from VWR International (Fontenay-sous-Bois, France), saffron dye from Microm Microtech France (Brignais, France), methanol (MeOH, ≥ 99.8%), dichloromethane (DCM, ≥ 99.9%), anhydrous tetrahydrofuran (THF, ≥ 99.9%), and erythrosin extra bluish from Sigma-Aldrich (St-Quentin Fallavier, France). Physiological serum was purchased from Ecoflac® B. Braun (Saint-Cloud, France). Phosphate-buffered saline (PBS), was purchased from Invitrogen (Cergy Pontoise, France). THF was dried using a PureSolv™ Micro Single Unit (Inert®) system.

2.2. Synthesis

The PLA_{50}-*b*-PEG-*b*-PLA_{50} triblock copolymer was synthesized following a previously described procedure [55]. For synthetic and characterization details please refer to the cited reference. In this work, the copolymer was obtained with a yield of 90%. The polymerization degree (DP) of each PLA block was calculated based on the EG/LA ratio of the ethylene oxide and the lactyl units calculated from ^{1}H NMR spectrum and equation (1):

(1) $$DP_{PLA}(\%) = \frac{1}{2} \times \frac{DP_{PEG}}{\frac{EG}{LA}}$$

Consequently, the overall molecular weight of the synthesized triblock copolymers was calculated using equation (2):

(2) $M_{ntriblock}(\%) = 2 \times (DP_{PLA} \times 72) + M_{nPEG}$

In this work, considering $M_{n\ PEG\ theoretical}$ = 20 000 g.mol^{-1} for the PEG central block and LA/EG=9/1 as determined by ^{1}H NMR analyses, the calculated average molecular weight was $M_{n\ NMR}$ = 320 000 g.mol^{-1} for PLA$_{50}$-*b*-PEG-*b*-PLA$_{50}$ with $M_{n\ PLA50\ NMR}$ = 175 000 g.mol^{-1} for each PLA$_{50}$ side block.

Poly(ε-caprolactone-*co*-α-triiodobenzoate-ε-caprolactone) (PCL-TIB) was synthesized according to the procedure previously described using a post-polymerization functionalization of PCL by 2,3,5-triiodobenzoyl chloride (TIBC) [54]. Synthetic and characterization details are provided as *Supplementary data S1*. In this work, PCL-TIB$_{11}$ was obtained with a yield of 80% and 11% substitution with respect to CL units. $Mn_{\ SEC}$ = 24 000 g.mol^{-1}, dispersity Đ = 1.7.

2.3. Physicochemical characterizations

Degradation of the copolymer blend was monitored by size-exclusion chromatography (SEC) and ^{1}H NMR analyses. The average molecular weight (M_n) and the dispersity (*Đ*) of the polymers were determined by SEC using a Viscotek GPCmax autosampler system fitted two Viscotek LT5000L Mixed Medium columns (300 x 7.8 mm) and a Viscotek VE 3580 RI detector. The mobile phase was THF at 1 mL.min^{-1} flow and 30 °C. Typically, the polymer (20 mg) was dissolved in THF (2 mL) and the resulting solution was filtered through a 0.45-µm Millipore filter before injection of 20 µL of filtered solution. The M_n was expressed according to calibration using polystyrene standards. The ^{1}H NMR spectra were recorded at room temperature using an AMX300 Bruker spectrometer operating at 300 MHz. Deuterated chloroform was used as the solvent, and chemical shifts were expressed in ppm with respect to

tetramethylsilane (TMS). The thermal properties of the polymers were characterized by differential scanning calorimetry (DSC). The DSC measurements were carried out under nitrogen on a Perkin Elmer Instrument DSC 6000 Thermal Analyzer. The samples were subjected to a first heating scan from 30 °C to 110 °C (10 °C.min^{-1}) followed by a cooling ramp to -50 °C (10 °C.min^{-1}) followed by an isotherm at -50 °C (3 min) and a second heating ramp to 180 °C (10 °C.min^{-1}). The melting temperature (T_m) and the glass transition temperature (T_g) were measured on the second heating ramp.

2.4. Mechanical tests

The polymer mechanical properties were determined by performing tensile mechanical tests on dog-bone type of tensile specimens, with an MTS Criterion® electromechanical test machine, equipped with a 25 N cell force. In order to adhere to physiological experimental conditions, an experimental thermo-regulated tank filled with 0.9% sodium chloride solution was designed and used, as previously reported by us [39]. The saline solution was heated to a temperature of 37 ± 1 °C. Tests were carried out at 0, 1, 4, and 8 weeks of degradation. Beyond 8 weeks, the extent of the decline in the mechanical properties of the specimen precluded further testing.

Two types of mechanical tests were performed. First, cyclic loading tests that consisted of a load at two strain levels (5% and 10%) followed by an unload to zero strain, with a constant strain rate of 1% per second. Secondly, relaxation tests that consisted of a load at two strain levels (5% and 10%) with a strain rate of 1% per second, followed by a tensile relaxation test of 30 min each. Between the 5% strain and the 10% strain relaxation phases, an unload to zero strain and a 10 minute waiting period were carried out. The tangent modulus was calculated at two strain levels, 0 and 5% (0% corresponding to the Young's modulus), and they are denoted E and $E_{5\%}$. It was evaluated during loading. The moduli were evaluated on an interval of strain of 0.3, the beginning of the zone measurement was chosen so that the test specimen was taut,

and the residual deformation did not contribute to the measurement. The zone measurements were 0.1-0.4% and 3.7-4%, respectively, for the two levels. *E* was calculated by linear regression on each part of the stress/strain curves.

2.5. Preparation of implantable test samples and RIBS

Two types of implants were prepared, *i.e.* films for rat in vivo implantation versus stents (a tubular shape) for the studies of implantability in anatomical specimens. For all of the samples, blends were prepared from PLA_{50}-*b*-PEG-*b*-PLA_{50} ($M_{n\ NMR}$ = 320 000 $g.mol^{-1}$) and PCL-TIB_{11} ($M_{n\ SEC}$ = 24 000 $g.mol^{-1}$). The ratios of PCL-TIB_{11} and PLA_{50}-PEG-PLA_{50} were adjusted to yield a polymer blend containing 2.5 wt% of iodine, which corresponds to a 10 wt% weight ratio of PCL-TIB_{11} the in blend.

Polymer films with a target thickness of 0.6 mm (based on commercially available stents) were manufactured by solvent evaporation. A predefined quantity of polymer was solubilized in acetone, the solution was poured into a small dish and placed under an extractor hood for 36 h to allow evaporation. Removal of residual solvent removal was achieved by further drying under vacuum at 1.10^{-3} mbar for 3 days. A 0.5-mm thick film was obtained, and implants (corresponding to a dog-bone type tensile specimen of 40 x 6 x 0.5 mm^3) were then punched from it.

Resorbable internal biliary stents (RIBS) were obtained from the blend with an injection molding machine (MPT Europe, The Netherlands). After preheating the blend to 120-130 °C in an injection chamber, the melted blend was injected into a tubular mold containing an inner insert. The thickness of the tube was controlled by the dimensions of the insert. The tube was ultimately demolded after being cooled with nitrogen. The dimensions were selected based on

commercial silicone internal biliary stents (IBS) (3.5 mm external diameter, 150 mm length, and 0.5 mm thickness).

All of the implants were sterilized by gamma radiations (60 Co radiation sources, ARC-nucléart, CEA Grenoble, France) with gamma doses of 25 kGy in keeping with a previous study [56].

2.6. Experimental design: in vitro and in vivo degradation

The experimental design is illustrated in the *Supplementary data S2*. Samples were implanted in rats *(surgical procedure hereafter)* to evaluate the in vivo degradation. The radiological acquisitions, physicochemical characterization, and mechanical analyses were carried out at various time points. Each analysis was conducted on a minimum of 3 samples. The time points were: baseline, 1 week, 1 month, 2 months, 3 months, and 6 months. Additionally, histological analyses were performed at 3 months and 6 months post-implantation.

In parallel, an in vitro degradation study was carried out to compare it with the in vivo degradation data. Samples were placed in 20 mL test tubes in PBS at 37 °C within an agitator/incubator. The PBS was replaced weekly in order to keep the pH of the solutions stable. The physicochemical characterizations and the mechanical analyses were carried out at the same time points.

2.7. Animals and surgical procedures

All of the animal procedures conformed with French government guidelines and were performed under license number *#5612-2016060910392662v3* (for experimental and animal care facilities) from the French Ministry of Agriculture (Articles R214-117 to R214-127 published on March 31, 2017). This study was in compliance with the ARRIVE guidelines (Animal Research: Reporting in Vivo Experiments) [57], and it received formal approval from

the animal experimentation ethics committee of Grenoble, ("Comité d'éthique en expérimentation animale de Grenoble", National agreement n°012).

Seventeen male rats aged 7 weeks and weighing 250 – 300 g (Charles River, France) were housed in groups of 2 under standard laboratory conditions (12 h light/dark cycle with lights off at 8:00 p.m. and a controlled temperature of 22 ± 2 °C). Water and standard laboratory chow were provided ad libitum. For all of the experiments, rectal temperature was monitored and the rats were maintained at 37 ± 0.5 °C. Anesthesia was induced by the inhalation of 5% isoflurane (Abbott Scandinavia AB, Solna, Sweden), and maintained throughout all surgical and imaging procedures with 2% isoflurane through a facial mask in 50% air-50% oxygen.

The surgical procedures were performed under sterile conditions. A median laparotomy was performed and one of the implants was inserted into the peritoneal space in a left lateral position. The muscular abdominal wall and the skin were then separately sutured, and the animals were allowed to recover from the anesthesia. After surgery, the animals received a single subcutaneous injection of an analgesic (Rimadyl, 5 $mg.kg^{-1}$). The rats were sacrificed under anesthesia (inhalation of 5% isoflurane), by intracardiac injection of sodium pentobarbital (100 mg).

2.8. In vivo computed tomography (CT) imaging

In vivo degradation of the implants was evaluated non-invasively using dynamic computed tomography (CT) acquisitions. To that purpose, CT-scans were acquired at baseline, 1 week, 1 month, 2 months, and 3 months on a subset of 7 rats using a dedicated small-animal system (nanoScan CT, Mediso, Hungary). At 3 months, three rats were euthanized for the ex vivo evaluation of the implants, and an additional CT scan was performed at 6 months on the remaining four animals.

The animals were anesthetized with 2% isoflurane in a 1:1 mixture of air and oxygen, They were then placed on a heating pad and their respiratory rate was monitored continuously. For the acquisition parameters, a rapid CT scan was performed to image the entire abdomen and to locate the implant. A focused acquisition was then performed at the level of the implant using the following parameters: medium zoom, 720 projections and 300 ms per projection at 70 kVp. The acquisition was reconstructed using dedicated software with isotropic voxels of 0.14 mm (Nucline, Mediso, Hungary). For the image analysis, the implant was segmented semi-automatically using a connected thresholding algorithm and 600 Hounsfield Units (HU) as the minimum threshold to distinguish the implant from the soft tissues (Vivoquant, Invicro). The obtained volume-of-interest (VOI) was used to determine the volume of the implant, as well as the mean and the maximal signal intensity (HU). Moreover, the distribution of the signal intensity within the VOI was also visualized as a histogram.

2.9. Histological analyses

For the histological analyses, at 3 and at 6 months post-surgery, the animals were sacrificed, the abdomen was opened, and samples were harvested in monobloc with neighboring structures. The samples were fixed first in 10% formalin for 24 hours at 4 °C and then embedded in paraffin. To obtain cross-sections of the implant and the surrounding adipose tissue, the samples were sliced using a CTM6 coverslip microtome from Thermo Fischer Scientific (Waltham, MA USA) into 2-µm slices. The sections were deparaffinized and stained with Hematoxylin Eosin Saffron (HES) according to standard protocols on a Leica ST5020 automated slide stainer (Wetzlar, Germany), and then examined qualitatively by light microscopy, focusing particularly on inflammatory processes associated with the implant. The intensity and the spreading of the inflammation were evaluated by a single senior pathologist (HG).

2.10. Human cadaveric implantability tests

RIBS implantability tests on the human bile duct were performed on cadavers by four experienced liver transplant gastrointestinal surgeons.

Formalin-fixed cadavers for anatomical dissection were selected from the Anatomy Laboratory, Faculty of Medicine, Grenoble, France (Laboratoire d'Anatomie Des Alpes Françaises). The cadavers had been embalmed with a formalin solution (ARTHYL) injected into the carotid artery and drained from the jugular vein, and then preserved in a refrigerated room. All of the tests were performed in compliance with the French regulations for post-mortem testing, and the protocol was approved by a local scientific committee of the Grenoble Alpes University.

A subcostal laparotomy was performed, with a main bile duct anterior approach. After a bile duct radial section, biliary reconstruction was performed using a standardized duct-to-duct biliary reconstruction by means of an end-to-end choledoco-choledocostomy. The posterior side of the biliary anastomosis was generated with a 6/0 polydioxanone running suture, and the anterior side with 6/0 polydioxanone interrupted sutures. A RIBS was inserted after construction of the posterior anastomotic suture. The stent length was tailored to bridge the entire common bile duct from the papilla to the hilar bifurcation.

The subjective stiffness evaluation of RIBS compared to silastic IBS, the assessment of the ease of implantation, the surgical procedure used, and the overall assessment were evaluated by surgeons using a questionnaire (*provided as Supplementary data S5*).

RIBS implantation in human bile ducts and its visualization were then evaluated using CT scans of the anatomical samples.

2.11. Statistical analysis

All of the data are presented as means and the standard deviation. The statistical analysis was carried out using *X*LSTAT (Addinsoft, Japan). Data comprising multiple time points were evaluated by repeated-measures ANOVA followed by a Student's t-test. The volumes, as well as the mean and the maximum signal intensities determined by CT scans in vivo in rats, were compared from baseline using one-way ANOVA corrected for multiple comparisons by the Holm-Sidak method (GraphPad). A difference was considered to be statistically significant at $p < 0.05$.

3. RESULTS AND DISCUSSION

3.1. Characteristics of the PCL-TIB/PLA-PEG-PLA blends

The objective was to design a radiopaque RIBS and to evaluate its properties during both in vitro and in vivo degradation. For this purpose, we selected a blend of PCL-TIB used as a degradable macromolecular contrast agent, and a PLA/PEG copolymer that has a long track record as an implantable biomaterial. More specifically, PLA_{50}-*b*-PEG-*b*-PLA_{50} triblock was selected for RIBS development as in previous studies it exhibited mechanical and degradation properties corresponding to the RIBS specifications (flexibility after drying, moderate Young's modulus, and an estimated in vivo degradation time of approximately 6 months for full resorption) [39,40]. PCL-TIB was selected as a radiopaque macromolecular additive due to its demonstrated ability to generate homogeneous blends with PLA/PEG copolymers and to generate radiopacity even at low percentages of iodine in the blends. Radiopaque PCL-$TIB_{3,5}$/PLA_{50}-*b*-PEG-*b*-PLA_{50} blends with as low as 2.5 wt% iodine resulted in good X-ray visualization in a preliminary study [54]. To achieve this iodine content, the blends contained 25 wt% of PCL-$TIB_{3,5}$. Such a high ratio of low-molecular weight PCL-TIB in the blend may, however, impact the mechanical and degradation properties of the targeted RIBS. For this reason, in the present work, we opted for a PCL-TIB with a higher degree of substitution.

The polymers were synthesized according to well-established procedures described in the Methods section. The molecular weight of the synthesized PLA_{50}-*b*-PEG-*b*-PLA_{50} triblock copolymer was firstly determined by ^{1}H NMR spectroscopy. The $M_{n\ NMR}$ was 320 000 g.mol^{-1}, which is in good agreement with the expected value ($M_{n\ theoretical}$ = 300 000 g.mol^{-1}). By contrast, the SEC analyses yielded molecular weight values that were approximately two times lower than those determined based on NMR, with an average molecular weight $M_{n\ SEC}$ = 90 000 g.mol^{-1}. This difference can be explained by the use of polystyrene standards for the SEC calibration, thus resulting in inaccurate measurements with aliphatic polyesters [58,59]. Moreover, the amphiphilic nature of the copolymers can modify their hydrodynamic volume and increase their retention time, thereby resulting in underestimated values. For PCL-TIB, the post-polymerization reaction conditions were optimized to increase the degree of substitution of the PCL backbone *(see Supplementary data S1 for a detailed synthetic protocol)*. A degree of substitution of 11% of TIB relative to the CL units was calculated based on the NMR analyses in accordance with our previous work by comparing the integrations of the signals in the range of 7.4-8.3 ppm corresponding to the aromatic protons of TIB with the integration of the proton at 4.0 ppm corresponding to the methylene group of PCLs. An average molecular weight $M_{n\ SEC}$ = 24 000 g.mol^{-1} with dispersity Đ = 1.7 was obtained by the SEC analysis.

The two polymers were then blended to achieve an iodine content of 2.5 wt%. This was achieved with only 10 wt% of PCL-TIB_{11} in the blend (**Figure 1)**. The impact of the RIBS injection molding technique on the molecular weight and the blend composition was limited. After injection molding, the average number molecular weight Mn was 90% of its initial value, the *Đ* decreased from 2.25 to 2.05, and the monomer unit ratios LA/EG and LA/CL remained largely unchanged after injection molding, with values corresponding to 99% and 90% of the initial ratios, respectively *(Supplementary data S7)*.

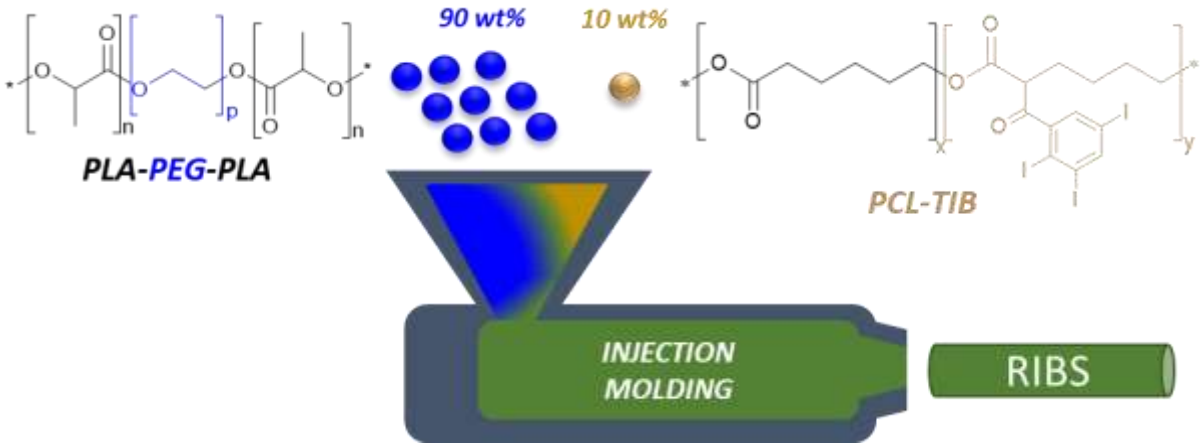

Figure 1: Schematic representation of the RIBS production.

Preliminary tests for the preparation of film tests confirmed that this polymer mix was able to form homogeneous films with no visible phase separation. This was also the case for the extruded RIBS, as shown in **Figure 5D**.

Differential scanning calorimetry analyses were performed on the blends processed by film evaporation and injection. Thermograms of the blends were similar irrespective of the processing method, with a single thermal transition observed at 42 °C corresponding to the glass transition of the amorphous PLA_{50}-*b*-PEG-*b*-PLA_{50} that represents 90 wt% of the blend (*Figure S8*). Variations of the heat capacity were in the same range, with $\Delta Cp \sim 0.4$ J/g.°C for PLA_{50}-*b*-PEG-*b*-PLA_{50} and $\Delta Cp \sim 0.35$ J/g.°C for the blends. These results ensure that in the context of this work, the processing method (film evaporation vs. injection) does not alter the thermal properties or the crystallinity of the samples, and therefore that the choice of samples (film or tube) does not impact the degradation studies.

In addition, at this iodine content, PCL-TIB/PLA_{50}-*b*-PEG-*b*-PLA_{50} was found to be cytocompatible under the conditions recommended by International and European standards (ISO 10993-5:2009) using a murine fibroblast proliferation assay *(the protocol and the results are provided as Supplementary data S4)*. This result confirms that PCL-TIB/PLA_{50}-*b*-PEG-*b*-

PLA_{50} may be suitable for the growth of fibroblasts and cell-contact applications and that it can be used to design of X-ray-visible medical devices

3.2. Rat implantation and animal tolerance

In order to conduct a comparative in vitro *vs.* in vivo study of the polymer degradation and of the change in the mechanical properties, flat samples in the shape of dog-bone type tensile specimens were first prepared from the blend using the readily reproducible solvent evaporation technique. Following careful removal of the residual traces of solvent, specimens were punched out from the films and sterilized prior to implantation. The specimens were implanted in 17 male rats in the peritoneal space in the left lateral position. All 17 implant samples were well-tolerated, as further confirmed by the histological analyses (see the corresponding paragraph). All of the 17 rats exhibited mild wound reactions surrounding the incision that resolved a few days after the surgery, and they did not exhibit postoperative pain. There were no signs of parietal or wound infections during the postoperative follow-up and no premature deaths.

3.3 In vitro vs. in vivo degradation study

Degradation of the copolymer blend was followed by size exclusion chromatography and ^{1}H NMR analyses. In terms of the molecular weight, the same trend was observed in vitro and in vivo, with a fast and quasi-linear molecular weight decrease during the first 10 weeks before stabilization at approximately 15% of the initial value (a Mw of approximately 20 000 $g.mol^{-1}$) (**Figure 2A**). The dispersity increased slightly until the 10^{th} week before stabilization at Đ~2.3. The composition of the copolymer blend changed during the degradation, with again similar trends observed in vitro and in vivo (**Figure 2B**). The LA/EG monomer unit ratio remained nearly constant over the course of the degradation study, without a statistically significant difference from baseline. This was not the case for the LA/CL ratio, with an initial value of

12.5 that then decreased drastically after 15 weeks to levels below 1 ($p < 0.0001$) *(the degradation measurements data and the statistical analyses are provided as Supplementary data S6)*.

This combined information suggests the following degradation scenario. During the first 10 weeks, in accordance with the reported slow degradation of PCL, only the PLA-*b*-PEG-*b*-PLA copolymer degraded. The contribution of the PCL-TIB in the molecular weight distribution was not noticeable under the conditions used to study the degradation due to the rather large dispersity of the triblock ($Đ = 1.64$) and the low content of PCL-TIB (10 wt%) in the blend. In parallel, the overall composition did not change as a result of the low, if any, diffusivity of the degraded PLA-*b*-PEG-*b*-PLA chains for which the molecular weights were still above 20 000 $g.mol^{-1}$. After 10 weeks, the molecular weight leveled off at 20 000 $g.mol^{-1}$, which corresponded to the molecular weight of the central PEG block and of PCL-TIB, whereas the LA/CL ratio decreased due to the diffusion of the PLA oligomers.

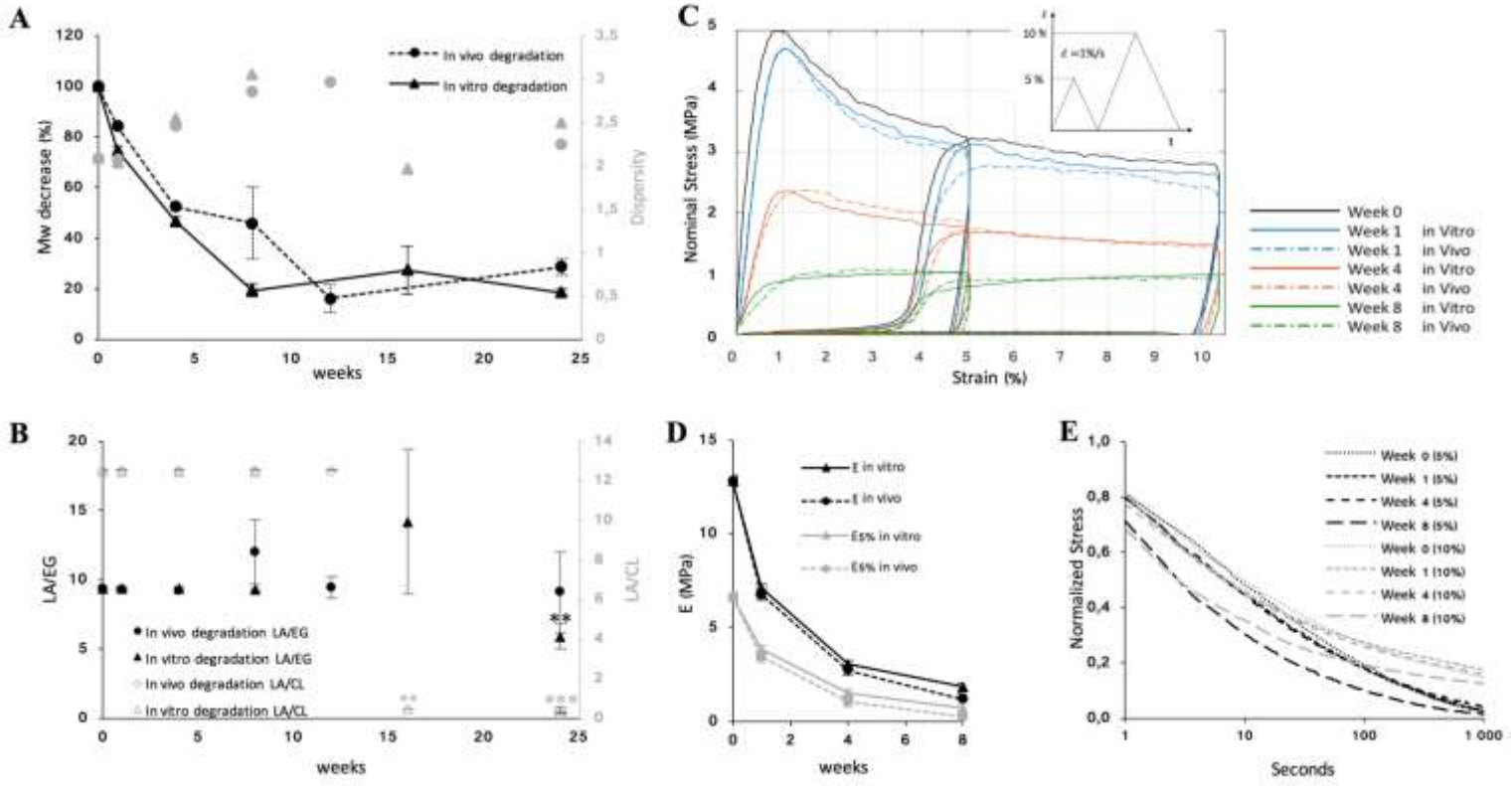

Figure 2:
Comparative study of the degradation of PCL-TIB$_{11}$/PLA-*b*-PEG-*b*-PLA in vivo (in rat intraperitoneal cavity, dotted line & round markers) or in vitro (PBS at 37 °C, solid line & triangular markers).
A. Changes in the molecular weight (M_w) (black lines) and the dispersity (Đ) (grey markers), * *and* ** *p < 0.05 and p < 0.01 in vivo vs. in vitro, respectively.*
B. Changes in the LA/EG monomer unit ratio (full black markers) and the LA/CL monomer unit ratio (empty grey markers), ** *and* *** *p < 0.01 and p < 0.0001 vs. baseline, respectively.* The data are expressed as means ± the SD and correspond to measurements with n = 4.
C. Stress–strain curves for cyclic loading tests at 0, 1, 4, and 8 weeks of degradation.
D. Young's modulus E and $E_{5\%}$ during degradation, comparison between the in vitro and the in vivo degradation.
E. Normalized relaxation test during in vivo degradation, 5% and 10% strain load.

In summary, up to 10 weeks, the samples contained degraded PLA-*b*-PEG-*b*-PLA chains and PCL-TIB, and the degradation of PLA-*b*-PEG-*b*-PLA was not advanced enough to impact the overall composition. After 10 weeks, the diffusion of the shortest PLA segments and of the more hydrophilic PLA-*b*-PEG residues left the samples enriched in PCL-TIB, thus explaining the decrease in the LA/CL ratio. In parallel, the small population of less degraded and more

hydrophobic PLA-*b*-PEG-*b*-PLA chains that were still present in the samples explains the stable LA/EG ratio.

3.4. Evolution of the mechanical properties

Figure 2C presents the stress–strain curves of the material submitted to the cyclic loading tests from zero to eight weeks. With the initial load, the stress first increased between 0 and 1% strain up to the maximum stress, and then decreased during the rest of the load.

In the course of degradation, the long polymeric chains were cleaved, leading to a decrease in the molecular weight and a decline in the mechanical properties. The shape of the curves changed and the stress decreased for any strain. After 8 weeks, the polymer had lost nearly 80% of its initial molecular weight, making further mechanical testing impossible to perform due to the extreme brittleness of the specimens.

The Young's modulus (*E*) and the modulus after a 5% strain cycle at each degradation time were measured. The results are presented in **Figure 2D**. The stiffness of the material appeared to decrease exponentially until 8 weeks, which is similar to the decline in the molecular mass (**Figure 2A**). Interestingly, a similar change was observed for both the in vivo and the in vitro degradation. No significant difference was noted, with overlapping standard deviations.

The viscoelastic properties of the material were further studied by means of the relaxation analysis, **Figure 2E** presents the results for the normalized relaxation test during the in vivo degradation, at 5 and 10% strain load, respectively, defined as:

(3) $$\sigma_{nr} = \frac{\sigma_{relax}}{\sigma_m} = \frac{\sigma_{relax}}{\sigma_{relax}(t=0)}$$

with σ_m being the static stress reached at the end of the load and σ_{relax} the stress recorded during relaxation at any time *t*.

The normalized curves for relaxation at 5% and 10% were nearly similar during the first 4 weeks of degradation for the two values of maximal strain. In other words, this indicates that

the temporal viscous component of the mechanical behavior was invariant during the early stages of the degradation. This means that, during this period, only the instantaneous elastic properties degraded. A number of changes in the normalized relaxation curves were observed from week 8 onward, which corresponds to the time when the specimens became very difficult to test.

Overall, the mechanical tests showed that the viscoelastic properties of the material were stable during the first 8 weeks, whereas the stiffness of the material decreased by approximately 70% after 4 weeks. Despite this rapid decrease in the degree of stiffness, the PCL-TIB/PLA_{50}-*b*-PEG-*b*-PLA_{50} blend can be further considered for RIBS as its initial mechanical properties are approximately10 times higher than those of biliary duct [39,60]. This should ensure that the mechanical properties of the RIBS remain high enough after 4 weeks to avoid anastomotic stricture and hence keep the tube lumen open, thus preventing biliary obstruction.

Mechanical tests before and after 25 kGy gamma radiation were performed (*Supplementary data S9)* to measure the impact of radiation-related degradation on the mechanical properties. The Young's modulus and the modulus after a 5% strain cycle were measured. A large difference was observed for the Young's modulus, but only 16% variation was observed after a 5% strain cycle. The form of the cycles was similar for the two specimens, meaning that the viscoelastic properties were not affected by the radiation. In fact, for the radiation only, the irradiation mainly affected the initial modulus of elasticity of the material, probably due to the breaking of bonds in the material. But after mechanical loading, the effects of loading or the irradiation may become similar, thereby leading to very similar mechanical behaviors.

3.5. Computed tomography imaging in rats

The samples implanted in rats could be clearly visualized upon CT imaging at all time points **(Figure 3,** *Supplementary data S3***)**, thus confirming that the selected radiopaque copolymer

blend allows efficient follow-up of the modifications of the morphology and the volumes of the samples due to the degradation process. More specifically, from baseline up to 3 months, no significant change was observed by CT scan imaging quantification (**Figure 3A-C**). Indeed, the volume and the mean signal intensity were of 75 ± 9 mm^3 and $1{,}037 \pm 155$ HU, respectively, at baseline, and similar values were observed at 3 months (74 ± 14 mm^3 and 967 ± 89 HU, respectively). It was noticed, however, that, at 3 months, the shape of the implant appeared to be more compact and rounded than at the earlier time points (**Figure 3D**). At 6 months, the implants appeared to be fragmented (Figure 3D, red and green colors). Even when considering the sum of the fragments, the volume was significantly reduced in comparison to baseline (47 ± 5 mm^3, $p < 0.01$) (**Figure 3A**). Moreover, the mean ($1{,}386 \pm 154$ HU, $P < 0.01$) but even more so the maximum signal intensity ($4{,}556 \pm 707$ vs. $2{,}100 \pm 214$ HU at baseline, $p < 0.0001$) were found to be significantly increased (**Figure 3B-C**). These focal increases in signal intensity were readily visualized on CT scan images, and they were also readily identifiable on the volumes-of-interest (VOIs) histograms that represent the average signal distribution within the VOIs at a given time point (**Figure 3C-D**). Indeed, focal hypersignals were visible at 6 months both on the CT scans and on the distribution curve with voxels > 2,000 HU (**Figure 3 D**, gray area).

These results are consistent with the degradation analysis. Up to 3 months, the samples contained degraded PLA-*b*-PEG-*b*-PLA chains and PCL-TIB, and the degradation of PLA-*b*-PEG-*b*-PLA was not advanced enough to impact the implant volume. As can be seen in Figure 2B, the overall composition was the same during this period. From 3 to 6 months, the diffusion of the shortest PLA segments and of the more hydrophilic PLA-*b*-PEG residues left the samples enriched in PCL-TIB, as explained by the drop-in the LA/CL ratio in Figure 2B. This explains the implant fragmentation and the loss of volume. The focal gains in signal intensity were, therefore, due to the increased concentration of PCL-TIB in the remaining fragments.

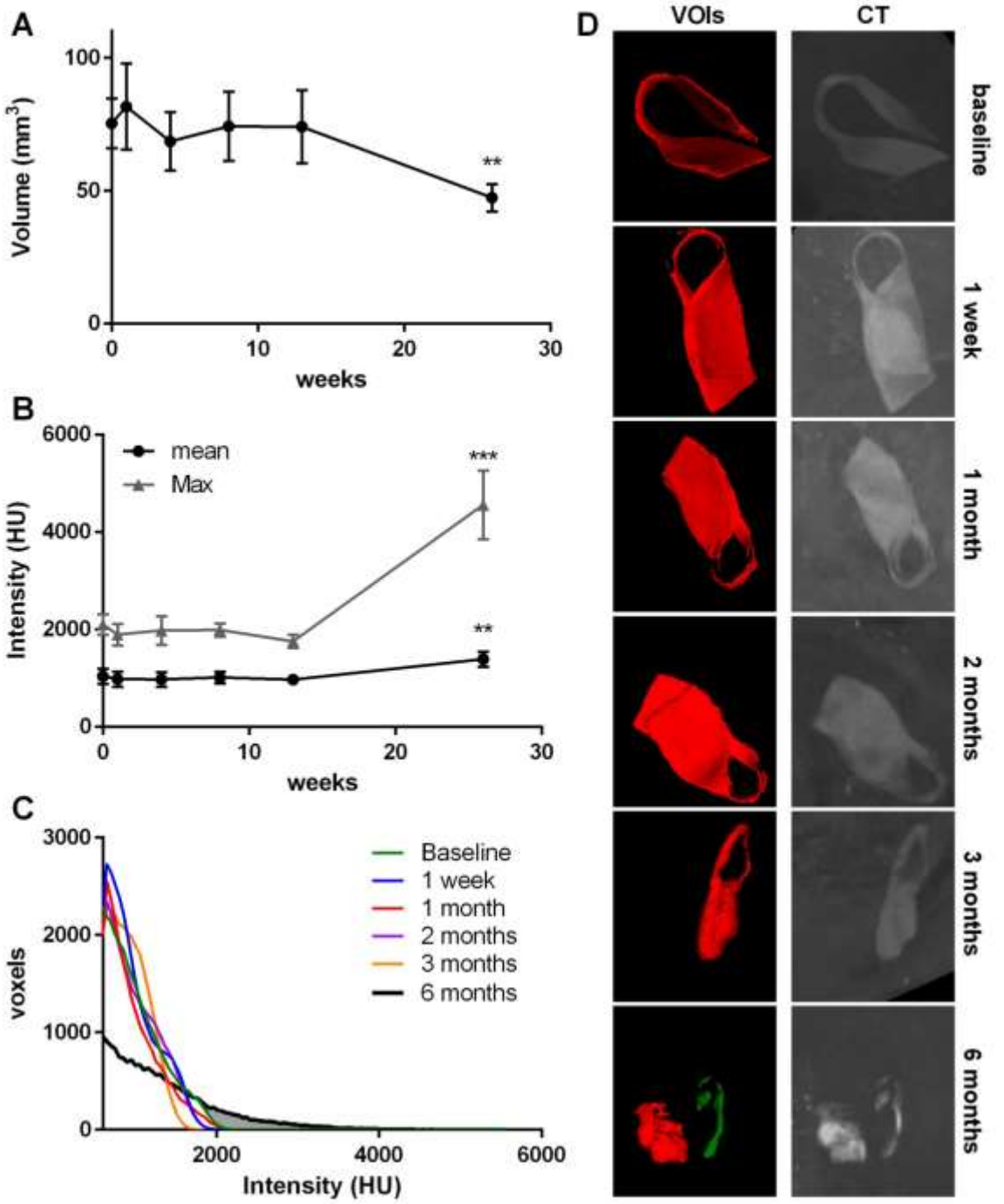

Figure 3: Computed tomography imaging. A. The volume of the implant from baseline to 6 months. B. The mean and the maximum signal intensities from baseline to 6 months. C. The average signal distribution within the VOIs at a given time point. All of the quantifications were performed based on the VOIs. D. CT scan appearance of the implants over time from the same animal (D-left: volume rendering of the VOIs obtained by semi-automated segmentation of the CT scans, D-right: CT scans scaled from -1,000 to 5,000 HU). *HU: Hounsfield unit; VOIs: Volumes-of interest; CT: Computed tomography. ** and *** $p < 0.01$ and $p < 0.0001$ vs. baseline, respectively.*

3.6. Histological results

Histopathological examinations of the implants were performed at 3 and 6 months post-surgery by a senior pathologist (HG). All of the samples were removed and analyzed in monoblock with the neighboring adipose structures. At 3 months (**Figure 4A**), despite a degree of degradation at the macromolecular level, the exogenous material was intact, surrounded by a thin fibrotic line and bordered by a small number of multinucleated giant cells, but without any inflammatory reaction.

At 6 months (**Figure 4B-C**), the exogenous material was fragmented, resorbed by a histiocytic and giant cell reaction, with a small number of lymphoplasma cells. This reaction was mild, restricted, and circumscribed, and it had not spread to the adjacent adipose tissue, nor was there any chronic inflammation or intense fibrosis. As was the case for the radiological observations, the material was found to be fragmented at 6 months of degradation. This observation is in agreement with the degradation scenario reported in this work, with most of the PLA-*b*-PEG blocks undergoing considerable degradation, while the PCL-TIB fragments remained largely intact due to their longer degradation time. The tissue integration was good, with a minimal inflammatory reaction that was less pronounced than the inflammatory reaction noted for the resorption of sutures for example. This confirms that the PCL-TIB/PLA_{50}-*b*-PEG-*b*-PLA_{50} biomaterial selected for the proposed radiopaque RIBS is suitable for implantation in LT applications.

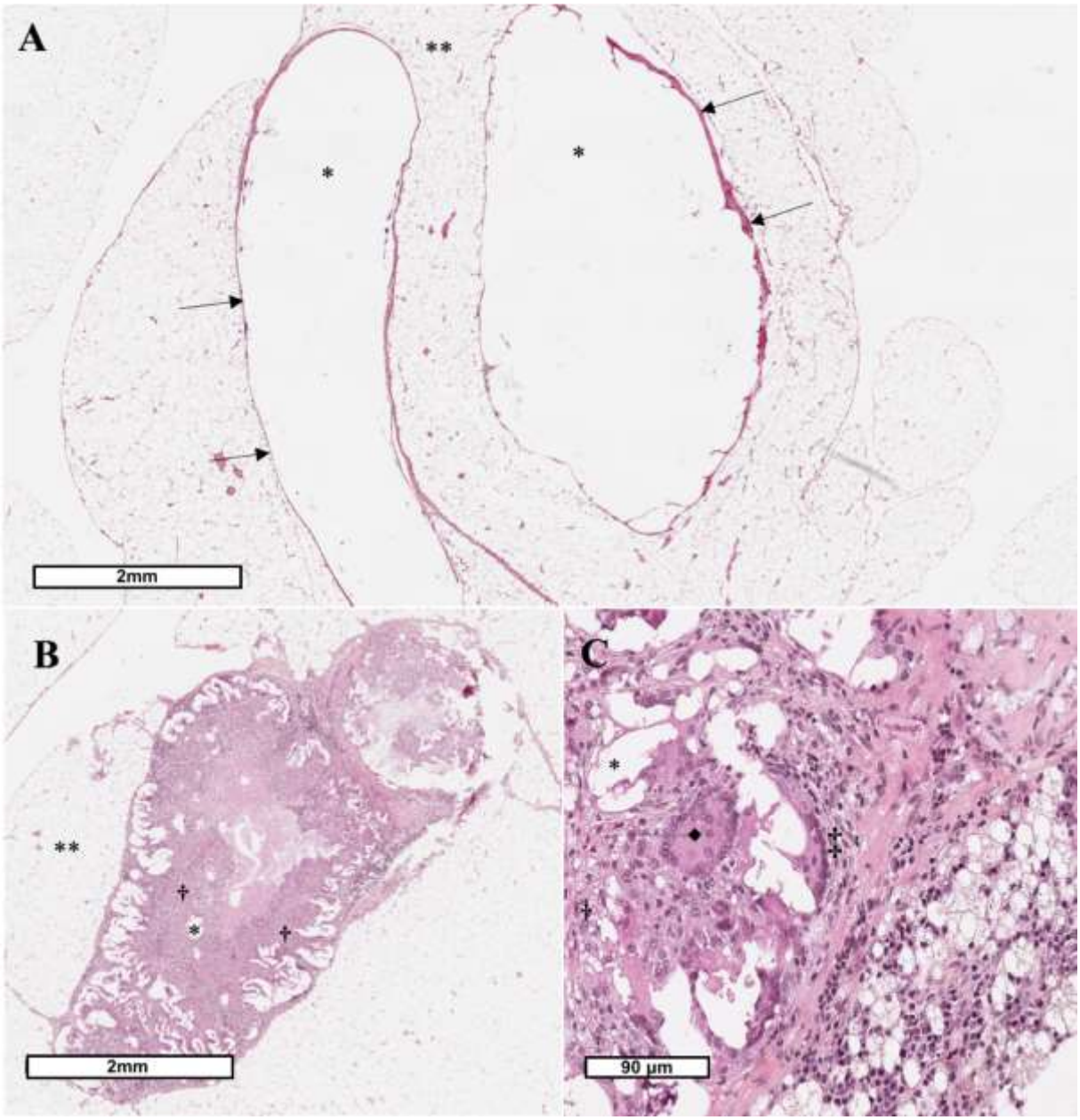

Figure 4: Histopathological examinations of the implanted stents with HES staining. A. At 3 months post-surgery (*2x magnification*). B. At 6 months post-surgery (*2x magnification*). C. At 6 months post-surgery (*200x magnification).*

→Fibrotic line, *Exogenous material, **Adipose tissue, †Histiocytic resorption, ‡Lymphoplasma cells, ◆Multinucleated cell.

3.7. Implantability in human bile ducts

The final aim of this work was to assess the implantability of the radiopaque RIBS and to confirm that they can be visualized using clinically relevant scanner. Four surgeons performed four anatomical dissections on human cadavers that exhibited no apparent abdominal pathologies or scars, a sex ratio of 1:1, and a median body mass index of 27 $kg.m^{-2}$. The implantability was assessed by means of a questionnaire that is provided in the *Supplementary data S6*.

For 25% of surgeons, the RIBS was too rigid compared to the silicone drain, which could increase the difficulty of implantation. The RIBS could readily be tailored, however, using surgical scissors in 100% of cases, and 75% of the surgeons succeeded in implanting the RIBS, thanks to a slightly modified biliary reconstruction technique. Thus, the usual technique was: first the posterior side of the biliary anastomosis made by a continuous suture, then the RIBS insertion, and finally the anterior side made by interrupted sutures. The relative stiffness of the RIBS compared to a silicone drain did not allow this usual technique to be performed. The modified technique is illustrated in **Figure 5A-C**. It consisted of making a posterior side with interrupted sutures by threading the sutures without tying them off, followed by insertion of the RIBS and tying the sutures to it. The anterior side was then performed as usual. This technique did not necessarily extend the operating time, nor is it expected to increase the risk of morbidity [61,62]. When the anastomosis was performed, the surgeon was satisfied in 100% of the cases. Seventy percent of them would use RIBS if they were available.

RIBS implantation in human bile ducts was evaluated using CT acquisition of the anatomical samples. The RIBS could readily be visualized in the images (**Figure 5E**), with sufficient density contrasting with the surrounding soft tissues. The RIBS were properly implanted, without bending, with an open lumen that allowed bile fluid circulation.

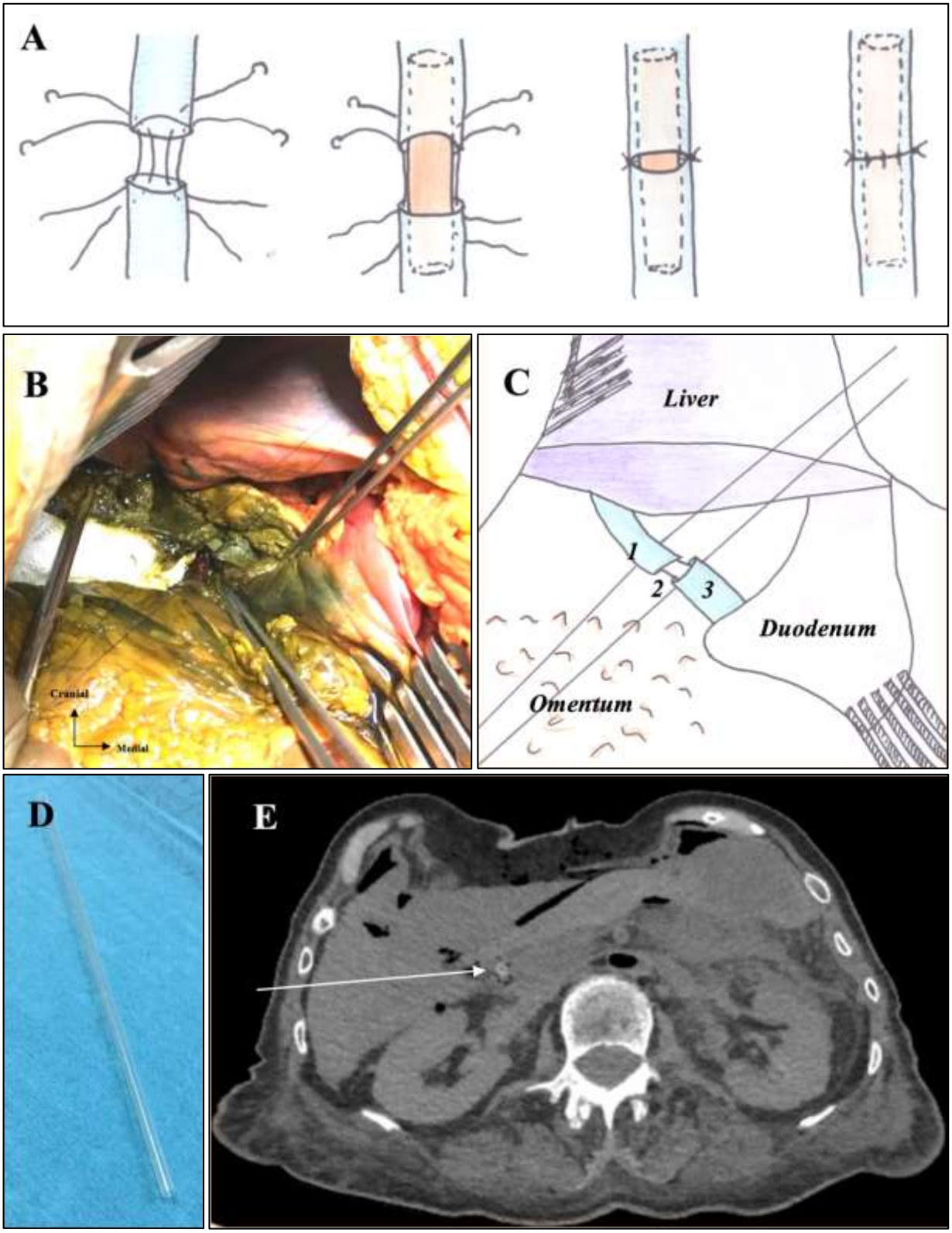

Figure 5:
A. Illustration of choledococholedostomy with RIBS implantation.
B. Intraoperative view of choledococholedostomy with RIBS implantation.
C. Schematic illustration of Figure B *(1. Proximal bile duct, 2. RIBS, 3. Distal bile duct)*.
D. RIBS prototype before implantation.
E. CT scan cross-section after implantation with RIBS visualization (white arrow).

CONCLUSION

In summary, we developed trackable RIBS and we validated the feasibility of its implantation in human bile duct for LT. This was achieved by blending and processing PLA_{50}-*b*-PEG-*b*-PLA_{50} as the RIBS main component and PCL-TIB as a macromolecular radiopacifier additive. Specifically, a polymer blend of PLA_{50}-*b*-PEG-*b*-PLA_{50} / PCL-TIB (90:10 w:w) yielded RIBS with suitable initial mechanical properties that exhibit stable radiopacity for CT scan visualization of the implant throughout its degradation. No significant difference was noted between the progression of the in vivo and the in vitro degradation. Mechanical tests showed that the viscoelastic properties of the material essentially did not change during the first 8 weeks, which matches the healing time required for the LT application. Histological observations indicated a rate of degradation compatible with human implantation, without major chronic inflammation or significant fibrosis. Finally, the post-mortem evaluation of human implantability and imaging of the RIBS prototype in human cadavers demonstrated the feasibility of using RIBS in human bile ducts for liver transplantation.

Acknowledgments

We thank the AFC (Association Française de Chirurgie) for financial support. J-P. Alcaraz (*SyNaBi*-TIMC-IMAG, Grenoble) and L. Cortella (CEA, Grenoble) for the gamma-ray sterilization experiments. The Plateforme Synbio 3 for the SEC analysis. P. Masson and P. Chaffanjon (LADAF, Grenoble) for cadaveric dissections and compliance with the post-mortem regulations. J. Abba, M. Chirica and O. Risse for the human bile duct implantations. The Radiology and Imaging Department of the Grenoble-Alpes University Hospital for the CT acquisitions of the anatomical specimens. This work was partly funded by France Life Imaging, grant “ANR-11-INBS-0006”.

REFERENCES

[1] T.H. Welling, D.G. Heidt, M.J. Englesbe, J.C. Magee, R.S. Sung, D.A. Campbell, J.D. Punch, S.J. Pelletier, Biliary complications following liver transplantation in the model for end-stage liver disease era: Effect of donor, recipient, and technical factors, Liver Transpl. 14 (2008) 73–80. https://doi.org/10.1002/lt.21354.

[2] D. Seehofer, D. Eurich, W. Veltzke-Schlieker, P. Neuhaus, Biliary Complications After Liver Transplantation: Old Problems and New Challenges, Am. J. Transplant. 13 (2013) 253–265. https://doi.org/10.1111/ajt.12034.

[3] N. Akamatsu, Y. Sugawara, D. Hashimoto, Biliary reconstruction, its complications and management of biliary complications after adult liver transplantation: a systematic review of the incidence, risk factors and outcome, Transpl. Int. Off. J. Eur. Soc. Organ Transplant. 24 (2011) 379–392. https://doi.org/10.1111/j.1432-2277.2010.01202.x.

[4] C. Goumard, M. Cachanado, A. Herrero, G. Rousseau, F. Dondero, P. Compagnon, E. Boleslawski, J.Y. Mabrut, E. Salamé, O. Soubrane, T. Simon, O. Scatton, Biliary reconstruction with or without an intraductal removable stent in liver transplantation: study protocol for a randomized controlled trial, Trials. 16 (2015) 598. https://doi.org/10.1186/s13063-015-1139-6.

[5] L. Grande, A. Pérez-Castilla, D. Matus, C. Rodriguez-Montalvo, A. Rimola, M. Navasa, J.C. García-Valdecasas, J. Visa, Routine use of the T tube in the biliary reconstruction of liver transplantation: is it worthwhile?, Transplant. Proc. 31 (1999) 2396–2397.

[6] S. Weiss, S.-C. Schmidt, F. Ulrich, A. Pascher, G. Schumacher, M. Stockmann, G. Puhl, O. Guckelberger, U.P. Neumann, J. Pratschke, P. Neuhaus, Biliary Reconstruction Using a Side-to-Side Choledochocholedochostomy With or Without T-Tube in Deceased Donor Liver Transplantation, Ann. Surg. 250 (2009) 766–771. https://doi.org/10.1097/SLA.0b013e3181bd920a.

[7] M. Wojcicki, P. Milkiewicz, M. Silva, Biliary tract complications after liver transplantation: a review, Dig. Surg. 25 (2008) 245–257. https://doi.org/10.1159/000144653.

[8] C. Riediger, M.W. Müller, C.W. Michalski, N. Hüser, T. Schuster, J. Kleeff, H. Friess, T-tube or no T-tube in reconstruction of the biliary tract during orthotopic liver transplantation - systematic review and meta-analysis, Liver Transpl. (2010) NA-NA. https://doi.org/10.1002/lt.22070.

[9] M. Shimoda, S. Saab, M. Morrisey, R.M. Ghobrial, D.G. Farmer, P. Chen, S.-H.B. Han, R.A. Bedford, L.I. Goldstein, P. Martin, others, A cost-effectiveness analysis of biliary anastomosis with or without T-tube after orthotopic liver transplantation, Am. J. Transplant. 1 (2001) 157–161.

[10] O. Scatton, B. Meunier, D. Cherqui, O. Boillot, A. Sauvanet, K. Boudjema, B. Launois, P.L. Fagniez, J. Belghiti, P. Wolff, D. Houssin, O. Soubrane, Randomized trial of choledochocholedochostomy with or without a T tube in orthotopic liver transplantation, Ann. Surg. 233 (2001) 432–437.

[11] G.C. Sotiropoulos, G. Sgourakis, A. Radtke, E.P. Molmenti, K. Goumas, S. Mylona, I. Fouzas, C. Karaliotas, H. Lang, Orthotopic Liver Transplantation: T-Tube or Not T-Tube? Systematic Review and Meta-Analysis of Results, Transplantation. 87 (2009) 1672–1680. https://doi.org/10.1097/TP.0b013e3181a5cf3f.

[12] F.C. Paes-Barbosa, P.C. Massarollo, W.M. Bernardo, F.G. Ferreira, F.K. Barbosa, M. Raslan, L.A. Szutan, Systematic review and meta-analysis of biliary reconstruction techniques in orthotopic deceased donor liver transplantation, J. Hepato-Biliary-Pancreat. Sci. 18 (2010) 525–536. https://doi.org/10.1007/s00534-010-0346-5.

[13] A. Amador, R. Charco, J. Martí, M. Navasa, A. Rimola, D. Calatayud, G. Rodriguez-

Laiz, J. Ferrer, J. Romero, C. Ginesta, C. Fondevila, J. Fuster, J.C. García-Valdecasas, Clinical trial on the cost-effectiveness of T-tube use in an established deceased donor liver transplantation program, Clin. Transplant. 21 (2007) 548–553. https://doi.org/10.1111/j.1399-0012.2007.00688.x.
[14] E. Girard, O. Risse, J. Abba, M. Medici, V. Leroy, M. Chirica, C. Letoublon, Internal biliary stenting in liver transplantation, Langenbecks Arch. Surg. (2018). https://doi.org/10.1007/s00423-018-1669-y.
[15] H. Tranchart, S. Zalinski, A. Sepulveda, M. Chirica, F. Prat, O. Soubrane, O. Scatton, Removable intraductal stenting in duct-to-duct biliary reconstruction in liver transplantation, Transpl. Int. 25 (2012) 19–24. https://doi.org/10.1111/j.1432-2277.2011.01339.x.
[16] M.W. Johnson, P. Thompson, A. Meehan, P. Odell, M.J. Salm, D.A. Gerber, S.L. Zacks, M.W. Fried, R. Shrestha, J.H. Fair, Internal biliary stenting in orthotopic liver transplantation, Liver Transplant. Off. Publ. Am. Assoc. Study Liver Dis. Int. Liver Transplant. Soc. 6 (2000) 356–361. https://doi.org/10.1053/lv.2000.5303.
[17] J.S. Barkun, G.N. Tzimas, M. Cantarovich, P.P. Metrakos, M. Deschênes, E. Alpert, S. Paraskevas, J.I. Tchervenkov, Do biliary endoprostheses decrease biliary complications after liver transplantation?, Transplant. Proc. 35 (2003) 2435–2437.
[18] S. Saab, Endoscopic Management of Biliary Leaks After T-Tube Removal in Liver Transplant Recipients: Nasobiliary Drainage Versus Biliary Stenting, Liver Transpl. 6 (2000) 627–632. https://doi.org/10.1053/jlts.2000.8200.
[19] J.M.P. Gursimran Kochhar Ibrahim A. Hanouneh, Mansour A. Parsi, Biliary complications following liver transplantation, World J. Gastroenterol. 19 (2013) 6. https://doi.org/10.3748/wjg.v19.i19.2841.
[20] B. Nemes, G. Gámán, A. Doros, Biliary complications after liver transplantation, Expert Rev. Gastroenterol. Hepatol. 9 (2015) 447–466. https://doi.org/10.1586/17474124.2015.967761.
[21] J.C. Middleton, A.J. Tipton, Synthetic biodegradable polymers as orthopedic devices, Biomaterials. 21 (2000) 2335–2346.
[22] J.L. Tokar, S. Banerjee, B.A. Barth, D.J. Desilets, V. Kaul, S.R. Kethi, M.C. Pedrosa, P.R. Pfau, D.K. Pleskow, S. Varadarajulu, A. Wang, L.-M. Wong Kee Song, S.A. Rodriguez, Drug-eluting/biodegradable stents, Gastrointest. Endosc. 74 (2011) 954–958. https://doi.org/10.1016/j.gie.2011.07.028.
[23] J. Li, J. Zhu, T. He, W. Li, Y. Zhao, Z. Chen, J. Zhang, H. Wan, R. Li, Prevention of intra-abdominal adhesion using electrospun PEG/PLGA nanofibrous membranes, Mater. Sci. Eng. C Mater. Biol. Appl. 78 (2017) 988–997. https://doi.org/10.1016/j.msec.2017.04.017.
[24] R. Rogacka, A. Chieffo, A. Latib, A. Colombo, Bioabsorbable and biocompatible stents. Is a new revolution coming?, Minerva Cardioangiol. 56 (2008) 483–491.
[25] M. Yaszemski, Evolution of bone transplantation: molecular, cellular and tissue strategies to engineer human bone, Biomaterials. 17 (1996) 175–185. https://doi.org/10.1016/0142-9612(96)85762-0.
[26] D.A. Brown, E.W. Lee, C.T. Loh, S.T. Kee, A New Wave in Treatment of Vascular Occlusive Disease: Biodegradable Stents—Clinical Experience and Scientific Principles, J. Vasc. Interv. Radiol. 20 (2009) 315–324. https://doi.org/10.1016/j.jvir.2008.11.007.
[27] X. Xu, T. Liu, S. Liu, K. Zhang, Z. Shen, Y. Li, X. Jing, Feasibility of biodegradable PLGA common bile duct stents: an in vitro and in vivo study, J. Mater. Sci. Mater. Med. 20 (2009) 1167–1173. https://doi.org/10.1007/s10856-008-3672-2.
[28] X. Xu, T. Liu, S. Liu, K. Zhang, Z. Shen, Y. Li, X. Jing, Feasibility of biodegradable PLGA common bile duct stents: an in vitro and in vivo study, J. Mater. Sci. Mater. Med. 20 (2009) 1167–1173.
[29] B. Meng, J. Wang, N. Zhu, Q.-Y. Meng, F.-Z. Cui, Y.-X. Xu, Study of biodegradable

and self-expandable PLLA helical biliary stent in vivo and in vitro, J. Mater. Sci. Mater. Med. 17 (2006) 611–617.
[30] J. Laukkarinen, I. Nordback, J. Mikkonen, P. Kärkkäinen, J. Sand, A novel biodegradable biliary stent in the endoscopic treatment of cystic-duct leakage after cholecystectomy, Gastrointest. Endosc. 65 (2007) 1063–1068. https://doi.org/10.1016/j.gie.2006.11.059.
[31] H. Tashiro, T. Ogawa, T. Itamoto, Y. Ushitora, Y. Tanimoto, A. Oshita, H. Amano, T. Asahara, Synthetic bioabsorbable stent material for duct-to-duct biliary reconstruction, J. Surg. Res. 151 (2009) 85–88. https://doi.org/10.1016/j.jss.2008.02.056.
[32] S. Tara, H. Kurobe, K.A. Rocco, M.W. Maxfield, C.A. Best, T. Yi, Y. Naito, C.K. Breuer, T. Shinoka, Well-organized neointima of large-pore poly(L-lactic acid) vascular graft coated with poly(L-lactic-co-ε-caprolactone) prevents calcific deposition compared to small-pore electrospun poly(L-lactic acid) graft in a mouse aortic implantation model, Atherosclerosis. 237 (2014) 684–691. https://doi.org/10.1016/j.atherosclerosis.2014.09.030.
[33] T.B. Wissing, V. Bonito, C.V.C. Bouten, A.I.P.M. Smits, Biomaterial-driven in situ cardiovascular tissue engineering-a multi-disciplinary perspective, NPJ Regen. Med. 2 (2017) 18. https://doi.org/10.1038/s41536-017-0023-2.
[34] L.C. Lins, F. Wianny, S. Livi, I.A. Hidalgo, C. Dehay, J. Duchet-Rumeau, J.-F. Gérard, Development of Bioresorbable Hydrophilic-Hydrophobic Electrospun Scaffolds for Neural Tissue Engineering, Biomacromolecules. 17 (2016) 3172–3187. https://doi.org/10.1021/acs.biomac.6b00820.
[35] J. Du, H. Chen, L. Qing, X. Yang, X. Jia, Biomimetic neural scaffolds: a crucial step towards optimal peripheral nerve regeneration, Biomater. Sci. 6 (2018) 1299–1311. https://doi.org/10.1039/c8bm00260f.
[36] B. Bhaskar, R. Owen, H. Bahmaee, Z. Wally, P. Sreenivasa Rao, G.C. Reilly, Composite porous scaffold of PEG/PLA support improved bone matrix deposition in vitro compared to PLA-only scaffolds, J. Biomed. Mater. Res. A. 106 (2018) 1334–1340. https://doi.org/10.1002/jbm.a.36336.
[37] A. Leroy, B. Nottelet, C. Bony, C. Pinese, B. Charlot, X. Garric, D. Noël, J. Coudane, PLA-poloxamer/poloxamine copolymers for ligament tissue engineering: sound macromolecular design for degradable scaffolds and MSC differentiation, Biomater. Sci. 3 (2015) 617–626. https://doi.org/10.1039/C4BM00433G.
[38] C. Pinese, A. Leroy, B. Nottelet, C. Gagnieu, J. Coudane, X. Garric, Rolled knitted scaffolds based on PLA-pluronic copolymers for anterior cruciate ligament reinforcement: A step by step conception: ROLLED KNITTED SCAFFOLDS, J. Biomed. Mater. Res. B Appl. Biomater. 105 (2017) 735–743. https://doi.org/10.1002/jbm.b.33604.
[39] Q. Breche, G. Chagnon, G. Machado, E. Girard, B. Nottelet, X. Garric, D. Favier, Mechanical behaviour′s evolution of a PLA-b-PEG-b-PLA triblock copolymer during hydrolytic degradation, J. Mech. Behav. Biomed. Mater. 60 (2016) 288–300. https://doi.org/10.1016/j.jmbbm.2016.02.015.
[40] Q. Breche, G. Chagnon, G. Machado, B. Nottelet, X. Garric, E. Girard, D. Favier, A non-linear viscoelastic model to describe the mechanical behavior's evolution of biodegradable polymers during hydrolytic degradation, Polym. Degrad. Stab. 131 (2016) 145–156. https://doi.org/10.1016/j.polymdegradstab.2016.07.014.
[41] L. Jones, J. Moir, C. Brown, R. Williams, J. French, The novel use of a biodegradable stent placed by percutaneous transhepatic cholangiography for the treatment of a hepaticojejunostomy biliary leak following an extended left hepatectomy and pancreaticoduodenectomy, Ann. R. Coll. Surg. Engl. 96 (2014) e1–e3. https://doi.org/10.1308/003588414X13946184901326.
[42] G. Mauri, C. Michelozzi, F. Melchiorre, D. Poretti, M. Tramarin, V. Pedicini, L.

Solbiati, G. Cornalba, L.M. Sconfienza, Biodegradable biliary stent implantation in the treatment of benign bilioplastic-refractory biliary strictures: preliminary experience, Eur. Radiol. 23 (2013) 3304–3310. https://doi.org/10.1007/s00330-013-2947-2.
[43] A. Siiki, I. Rinta-Kiikka, J. Sand, J. Laukkarinen, Biodegradable biliary stent in the endoscopic treatment of cystic duct leak after cholecystectomy: the first case report and review of literature, J. Laparoendosc. Adv. Surg. Tech. A. 25 (2015) 419–422. https://doi.org/10.1089/lap.2015.0068.
[44] B.C. Thanoo, M.C. Sunny, A. Jayakrishnan, Tantalum-loaded polyurethane microspheres for particulate embolization: preparation and properties, Biomaterials. 12 (1991) 525–528.
[45] B.C. Thanoo, A. Jayakrishnan, Barium sulphate-loaded p(HEMA) microspheres as artificial emboli: preparation and properties, Biomaterials. 11 (1990) 477–481.
[46] F. Luderer, I. Begerow, W. Schmidt, H. Martin, N. Grabow, C.M. Bünger, W. Schareck, K.-P. Schmitz, K. Sternberg, Enhanced visualization of biodegradable polymeric vascular scaffolds by incorporation of gold, silver and magnetite nanoparticles, J. Biomater. Appl. 28 (2013) 219–231. https://doi.org/10.1177/0885328212443393.
[47] T. Lämsä, H. Jin, J. Mikkonen, J. Laukkarinen, J. Sand, I. Nordback, Biocompatibility of a new bioabsorbable radiopaque stent material (BaSO4 containing poly-L,D-lactide) in the rat pancreas, Pancreatol. Off. J. Int. Assoc. Pancreatol. IAP Al. 6 (2006) 301–305. https://doi.org/10.1159/000092772.
[48] I. Nordback, S. Räty, J. Laukkarinen, S. Järvinen, A. Piironen, J. Leppiniemi, M. Kellomäki, J. Sand, A novel radiopaque biodegradable stent for pancreatobiliary applications--the first human phase I trial in the pancreas, Pancreatol. Off. J. Int. Assoc. Pancreatol. IAP Al. 12 (2012) 264–271. https://doi.org/10.1016/j.pan.2012.02.016.
[49] J.L. Pariente, L. Bordenave, R. Bareille, C. Ohayon-Courtes, C. Baquey, M. Le Guillou, In vitro cytocompatibility of radio-opacifiers used in ureteral endoprosthesis, Biomaterials. 20 (1999) 523–527.
[50] Y. Wang, N.M.S. van den Akker, D.G.M. Molin, M. Gagliardi, C. van der Marel, M. Lutz, M.L.W. Knetsch, L.H. Koole, A Nontoxic Additive to Introduce X-Ray Contrast into Poly(Lactic Acid). Implications for Transient Medical Implants Such as Bioresorbable Coronary Vascular Scaffolds, Adv. Healthc. Mater. 3 (2014) 290–299. https://doi.org/10.1002/adhm.201300215.
[51] B. Nottelet, J. Coudane, M. Vert, Synthesis of an X-ray opaque biodegradable copolyester by chemical modification of poly (epsilon-caprolactone), Biomaterials. 27 (2006) 4948–4954. https://doi.org/10.1016/j.biomaterials.2006.05.032.
[52] C. Rode, A. Schmidt, R. Wyrwa, J. Weisser, K. Schmidt, N. Moszner, R.-P. Gottlöber, K. Heinemann, M. Schnabelrauch, Synthesis and processability into textile structures of radiopaque, biodegradable polyesters and poly(ester-urethanes): Radiopaque, biodegradable polyesters and poly(ester-urethanes), Polym. Int. 63 (2014) 1732–1740. https://doi.org/10.1002/pi.4707.
[53] K. Lei, Y. Chen, J. Wang, X. Peng, L. Yu, J. Ding, Non-invasive monitoring of in vivo degradation of a radiopaque thermoreversible hydrogel and its efficacy in preventing post-operative adhesions, Acta Biomater. 55 (2017) 396–409. https://doi.org/10.1016/j.actbio.2017.03.042.
[54] R. Samuel, E. Girard, G. Chagnon, S. Dejean, D. Favier, J. Coudane, B. Nottelet, Radiopaque poly(ε-caprolactone) as additive for X-ray imaging of temporary implantable medical devices, RSC Adv. 5 (2015) 84125–84133. https://doi.org/10.1039/C5RA19488A.
[55] A. Leroy, C. Pinese, C. Bony, X. Garric, D. Noël, B. Nottelet, J. Coudane, Investigation on the properties of linear PLA-poloxamer and star PLA-poloxamine copolymers for temporary biomedical applications, Mater. Sci. Eng. C Mater. Biol. Appl. 33

(2013) 4133–4139. https://doi.org/10.1016/j.msec.2013.06.001.
[56] S. El Ichi, A. Zebda, J.-P. Alcaraz, A. Laaroussi, F. Boucher, J. Boutonnat, N. Reverdy-Bruas, D. Chaussy, M.N. Belgacem, P. Cinquin, D.K. Martin, Bioelectrodes modified with chitosan for long-term energy supply from the body, Energy Environ. Sci. 8 (2015) 1017–1026. https://doi.org/10.1039/C4EE03430A.
[57] C. Kilkenny, W. Browne, I.C. Cuthill, M. Emerson, D.G. Altman, Animal Research: Reporting in vivo Experiments—The ARRIVE Guidelines, (n.d.) 3.
[58] A. Kowalski, A. Duda, S. Penczek, Polymerization of L , L -Lactide Initiated by Aluminum Isopropoxide Trimer or Tetramer, Macromolecules. 31 (1998) 2114–2122. https://doi.org/10.1021/ma971737k.
[59] M.-H. Huang, S. Li, M. Vert, Synthesis and degradation of PLA–PCL–PLA triblock copolymer prepared by successive polymerization of ε-caprolactone and dl-lactide, Polymer. 45 (2004) 8675–8681. https://doi.org/10.1016/j.polymer.2004.10.054.
[60] E. Girard, G. Chagnon, E. Gremen, M. Calvez, C. Masri, J. Boutonnat, B. Trilling, B. Nottelet, Biomechanical behaviour of human bile duct wall and impact of cadaveric preservation processes., J. Mech. Behav. Biomed. Mater. 98 (2019) 291–300. https://doi.org/10.1016/j.jmbbm.2019.07.001.
[61] S. Hirano, E. Tanaka, T. Shichinohe, O. Suzuki, K. Hazama, H. Kitagami, K. Okamura, T. Yano, S. Kondo, Treatment strategy for hilar cholangiocarcinoma, with special reference to the limits of ductal resection in right-sided hepatectomies, J. Hepatobiliary. Pancreat. Surg. 14 (2007) 429–433. https://doi.org/10.1007/s00534-006-1190-5.
[62] M. Kasahara, H. Egawa, Y. Takada, F. Oike, S. Sakamoto, T. Kiuchi, S. Yazumi, T. Shibata, K. Tanaka, Biliary reconstruction in right lobe living-donor liver transplantation: Comparison of different techniques in 321 recipients, Ann. Surg. 243 (2006) 559–566. https://doi.org/10.1097/01.sla.0000206419.65678.2e.

Supplementary data

From in vitro evaluation to human post-mortem pre-validation of a radiopaque and resorbable internal biliary stent for liver transplantation applications

Edouard GIRARD[1,2,3,*], Grégory CHAGNON[1], Alexis BROISAT[4,5], Stéphane DEJEAN[6] Audrey SOUBIES[4,5], Hugo GIL[7], Tahmer SHARKAWI[8], François BOUCHER[1,5], Gaël S ROTH[9], Bertrand TRILLING[1,2,3], Benjamin NOTTELET[6,*]

[1] Univ. Grenoble Alpes, CNRS, CHU Grenoble Alpes, Grenoble INP, TIMC-IMAG, F-38000 Grenoble, France

[2] Département de chirurgie digestive et de l'urgence, Centre Hospitalier Grenoble-Alpes, 38000 Grenoble, France

[3] Laboratoire d'anatomie des Alpes françaises (LADAF), UFR de médecine de Grenoble, Université de Grenoble-Alpes, F-38700 Grenoble, France.

[4] INSERM, Unité 1039, F-38000 Grenoble, France

[5] Radiopharmaceutiques Biocliniques, Université Grenoble-Alpes, F-38000 Grenoble, France

[6] IBMM, Université de Montpellier, CNRS, ENSCM, Montpellier, France

[7] Département d'anatomopathologie et cytologie, Centre Hospitalier Grenoble-Alpes, 38000 Grenoble, France

[8] ICGM, Université de Montpellier, CNRS, ENSCM, Montpellier, France

[9] Institute for Advanced Biosciences, INSERM U1209/CNRS UMR 5309, Université Grenoble-Alpes, F-38700 Grenoble, France

*** Corresponding authors:**

Dr Edouard GIRARD, Laboratoire TIMC-IMAG, Domaine de la Merci, 38706 La Tronche Cedex, France. E-mail address: edouard.girard@univ-grenoble-alpes.fr

Prof. Benjamin NOTTELET, Institut des Biomolécules Max Mousseron, UFR Pharmacie, 15 Avenue Charles Flahault, 34093 Montpellier cedex 05, France. Tel: +33 (0)411759697. E-mail address: benjamin.nottelet@umontpellier.fr

Content of supplementary data:

S1- Synthetic procedure for PCL-TIB

Typically, PCL (35 mmol of CL unit, 4 g) was dissolved in anhydrous THF (400 mL) in a four-necked reactor equipped with a mechanical stirrer and kept at -50 °C under argon atmosphere. A solution of LDA (0.5 eq./CL unit, 8.8 mL) was injected with a syringe through a septum and the mixture was kept at -50 °C under stirring for 30 min. After this activation step, TIBC (0.3 eq./CL unit, 5.6 g) was added, the mixture was kept under stirring for 30 min at a temperature raising from -50 °C to -30°C. The reaction was then stopped by addition of a saturated solution of NH_4Cl (300 mL) and pH was adjusted to 7 with 1M HCl. The polymer was extracted with dichloromethane (3 × 150 mL). The combined organic phases were washed three times with distilled water (3 × 150 mL), dried on anhydrous $MgSO_4$ and filtered. After partial solvent evaporation under reduced pressure, the polymer was recovered by two precipitations in cold methanol and dried overnight under vacuum. The polymer PCL-TIB_{11} was obtained with a yield of 80 % and 11 % substitution with respect to CL units.

^{1}H NMR: (300 MHz; $CDCl_3$) : δ (ppm) = 8.3 and 7.4-7.6 (2H, C*H*), 4.0 (2H, CH_2-O), 2.3 (2H, C(O)CH_2), 1.6 (4H, C(O)CH_2-CH_2-CH_2-CH_2-CH_2-O), 1.4 (2H, C(O)CH_2-CH_2-CH_2-CH_2-CH_2-O). $\overline{M_n}$ = 24 000 g.mol^{-1}, Đ = 1.7

S2- In vivo experimental design

Figure S2: Experimental design, provisional table of analyses

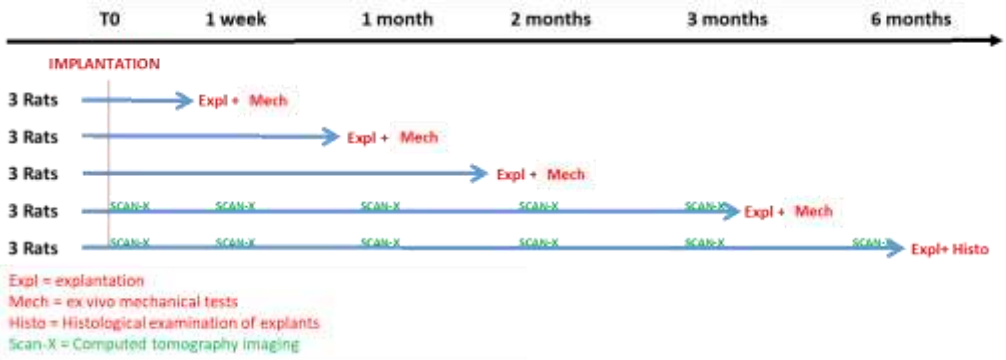

S3- Computed Tomography imaging in rats

Movie S3. Samples implanted in rats, CT imaging tri-dimensional visualization

S4- Preliminary evaluation of the blend cytocompatibility

Mouse L929 fibroblasts (L929) were cultured in modified Eagle's medium (MEM) containing 10% horse serum, penicillin (100 µg.mL^{-1}), streptomycin (100 µg.mL^{-1}), and glutamax (1%). Films were disinfected in ethanol for 30 minutes before being immersed in a solution of sterile PBS containing penicillin and streptomycin (1 mg.mL^{-1}) and incubated for 48 h at 37°C. The films were then rinsed 3 times with sterile PBS before being soaked for 12 hours in sterile PBS. These sterile films were stamped to fit the wells of 24-well cell culture plates. In vitro cytocompatibility was assessed by monitoring the proliferation of L929 fibroblasts on the surface of the plates. To do this, the films were placed in polystyrene 24-well tissue culture plates (TCPS) and seeded with 1×10^4 L929 cells. Cell viability after 1, 2 and 3 days was evaluated using the PrestoBlueTM assay that reflects the number of living cells present on a surface at a given time point. Culture medium was removed at scheduled time points and replaced by 1 mL of fresh medium containing 10% PrestoBlueTM. Fluorescence at λ = 530 nm (λex) and λ = 615 nm (λem) was measured on a Victor X3 photometer (Perkin Elmer). All data points and standard deviations correspond to measurements in triplicate.

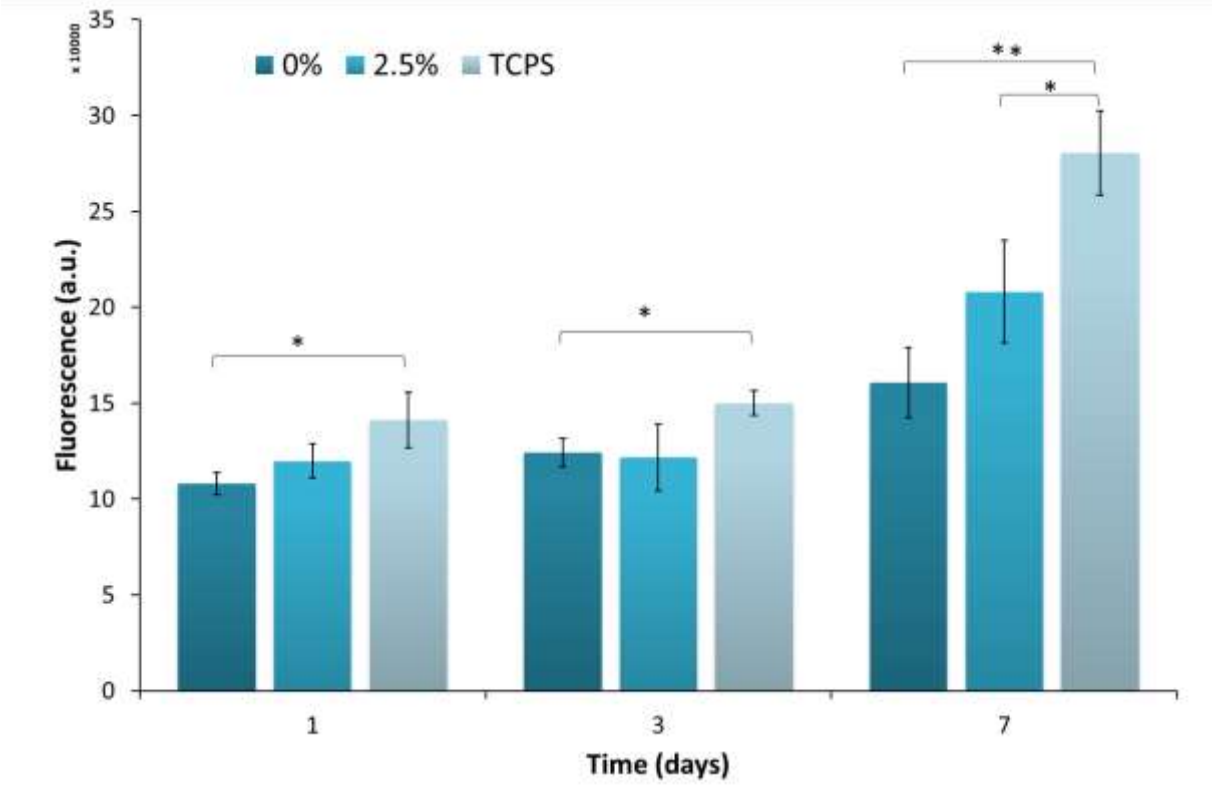

Figure S4. Preliminary cytocompatibility test. Proliferation at 1, 3 and 7 days of L929 murine fibroblasts on the radiopaque PCL-TIB/PLA$_{50}$-*b*-PEG-*b*-PLA$_{50}$ (2,5 wt% iodine) blends compared to pure PLA$_{50}$-*b*-PEG-*b*-PLA$_{50}$ (0 wt% iodine) and TCPS (Tissue Culture Polystyrene) positive control. (Student's t-test, a difference was considered to be statistically significant at $p<0.05$ (*) and $p<0.01$ (**).

S5- Questionnaire used to evaluate RIBS implantability

Post-mortem RIBS implantability				
	surgeon 1	**surgeon 2**	**surgeon 3**	**surgeon 4**
RIBS flexibility scale: -5=too soft, 0=ideal, +5= too rigid	4	3	1	0
RIBS thickness scale: -5=too thin, 0=ideal, +5= too thick	-3	0	0	-1
Flexibility and thickness can according to you:				
Make the implementation more difficult: 1=Yes, 0=No	1	1	0	0
Decrease the expected benefit of the drain: 1=Yes, 0=No	0	0	0	0
Potentially increase morbidity: 1=Yes, 0=No	1	0	0	0
Did you have trouble cutting the RIBS to the right size: 1=Yes, 0=No				
Has implantation been facilitated by RIBS warming: 1=Yes, 0=No	0	1	1	1
Do you think you have damaged the RIBS during implantation: 1=Yes, 0=No	1	0	0	0
Are you satisfied with your anastomosis: 1=Yes, 0=No	0	1	1	1
If no, for what reasons	RIBS folds			
Which anastomosis technique did you use?				
RIBS insertion after a posterior face realization by a continuous suture	1	0	0	0
around the RIBS with interrupted suture	0	1	1	1
Would you use this RIBS in common practice: 1=Yes, 0=No	0	1	1	1
If no, for what reasons	cf. comments. requires another technique, too time-consuming in my opinion			
Comments	Anastomosis should be performed around the RIBS, if the RIBS is inserts after the posterior face realization, it folds and risks being dysfunctional			

S6- ^{1}H NMR of the copolymers blend, degradation measurements data and statistical analyses

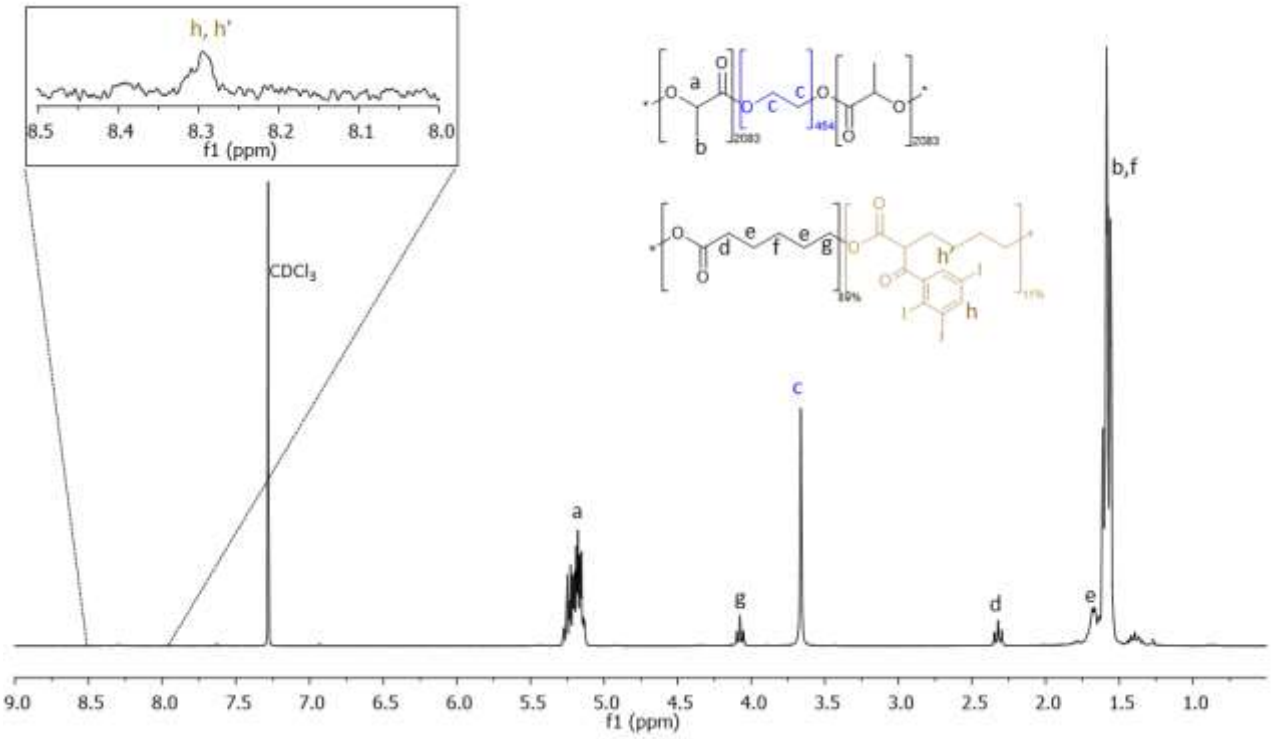

1H NMR spectrum of initial PCL-TIB$_{11}$/PLA$_{50}$-*b*-PEG-*b*-PLA$_{50}$ blend (10wt% PCL-TIB$_{11}$)

Raw data (SEC, NMR) of the degradation study

		SEC data			^{1}H NMR data*				
Time points	**In vivo or In vitro**	**Mn**	**Mw**	**D**	**1H PLA (5.2 ppm)**	**1H PCL (4.1 ppm)**	**1H PEG (3.6 ppm)**	**LA/EG**	**LA/CL**
0	before degradation	92755	203381	2.19	1	0.08	0.11	9.09	12.50
		89886	202679	2.25	1	0.08	0.11	9.09	12.50
		85999	202800	2.36	1	0.08	0.11	9.09	12.50
0	before degradation / after γ sterilization	47678	98778	2.07	1	0.08	0.1075	9.30	12.50
		47677	100810	2.11	1	0.08	0.1075	9.30	12.50
		47752	99855	2.09	1	0.08	0.105	9.52	12.50
1 w	in vitro	36931	75882	2.05	1	0.08	0.1075	9.30	12.50
		36541	75959	2.07	1	0.08	0.1075	9.30	12.50
		36257	72428	2	1	0.08	0.105	9.52	12.50
1 w	in vivo	41044	85751	2.09	1	0.08	0.1075	9.30	12.50
		39925	82991	2.08	1	0.08	0.11	9.09	12.50
		40493	83337	2.06	1	0.08	0.1075	9.30	12.50
4w	in vitro	16847	47778	2.84	1	0.08	0.1075	9.30	12.50
		17714	45164	2.55	1	0.08	0.1075	9.30	12.50
		20780	47053	2.26	1	0.08	0.105	9.52	12.50
4w	in vivo	21081	51979	2.47	1	0.08	0.11	9.09	12.50
		19756	51822	2.62	1	0.08	0.1075	9.30	12.50
		23288	53202	2.28	1	0.08	0.11	9.09	12.50
8w	in vitro	6432	20284	3.15	1	0.08	0.11	9.09	12.50
		6105	18341	3	1	0.08	0.1075	9.30	12.50
		6609	19678	2.98	1	0.08	0.1075	9.30	12.50
8w	in vivo	16894	53497	3.17	1	0.08	0.075	13.33	12.50
		19301	52986	2.75	1	0.08	0.075	13.33	12.50
		11596	30850	2.66	1	0.08	0.1075	9.30	12.50
16w	in vitro	20166	33328	1.65	1	0.36	0.115	8.70	2.78
		11549	24685	2.14	1	1.96	0.0675	14.81	0.51
		11342	23775	2.1	1	2.23	0.0525	19.05	0.45
12w	in vivo	4851	14308	2.95	1	0.08	0.1075	9.30	12.50
		6487	16047	2.47	1	0.08	0.115	8.70	12.50
		5105	17909	3.51	1	0.9	0.0975	10.26	1.11
24w	in vitro	7494	18937	2.53	1	3.4	0.16	6.25	0.29
		7289	17979	2.47	1	3.88	0.205	4.88	0.26
		7492	18564	2.48	1	3.67	0.1525	6.56	0.27
24w	in vivo	11541	28208	2.44	1	2.03	0.1575	6.35	0.49
		13726	30686	2.24	1	2.65	0.0825	12.12	0.38
		13155	27107	2.06	1	4.69	0.115	8.70	0.21

Statistical analysis

All data are presented as mean. Multiple time point data were evaluated by repeated measures ANOV. A difference was considered to be statistically significant at $p<0.05$.

^{1}H NMR data

LA/EG	1 week	4 weeks	8 weeks	12 or 16 weeks	24 weeks
in vitro	9.38	9.38	9.23	14.19	5.9
in vivo	9.23	9.38	11.98	9.42	9.06
p	0.23	1	0.11	0.19	0.15

LA/CL	1 week	4 weeks	8 weeks	12 or 16 weeks	24 weeks
in vitro	12.5	12.5	12.5	1.25	0.27
in vivo	12.5	12.5	12.5	8.7	0.36
p	1	1	1	0.13	0.35

LA/EG vs baseline	1 week	4 weeks	8 weeks	12 or 16 weeks	24 weeks
in vitro	9.38	9.38	9.23	14.19	5.9
baseline	9.38	9.38	9.38	9.38	9.38
p	1	1	0.23	0.18	0.0026
in vivo	9.23	9.37	11.99	9.42	9.05
baseline	9.38	9.38	9.38	9.38	9.38
p	0.23	1	0.12	0.93	0.86

LA/CL vs baseline	1 week	4 weeks	8 weeks	12 or 16 weeks	24 weeks
in vitro	12.5	12.5	12.5	1.25	5.9
baseline	12.5	12.5	12.5	12.5	12.5
p	1	1	1	0.0001	3.35E-12
in vivo	12.5	12.5	12.5	8.7	0.27
baseline	12.5	12.5	12.5	12.5	12.5
p	1	1	1	0.37	1.19E-08

SEC data

Mw	1 week	4 weeks	8 weeks	12 or 16 weeks	24 weeks
in vitro	74756	46665	19434	27263	18493
in vivo	84026	52334	45777	16088	28667
p	0.003	0.003	0.02	0.025	0.0007

Dispersity	1 week	4 weeks	8 weeks	12 or 16 weeks	24 weeks
In vitro	2.04	2.55	3.04	1.96	2.49
In vivo	2.08	2.46	2.86	2.98	2.25
p	0.18	0.66	0.33	0.04	0.09

S7- Impact of injection molding on the molecular weight and composition of the blend

Before injection				
SEC analysis			1H NMR analysis	
Mn	Mw	D	LA/EG	LA/CL
89 500	202 000	2,3	9	12,5

After injection				
SEC analysis			1H NMR analysis	
Mn	Mw	D	LA/EG	LA/CL
81 000	166 500	2,05	9	11,2

S8- Impact of the processing on the thermal properties of the copolymers blend

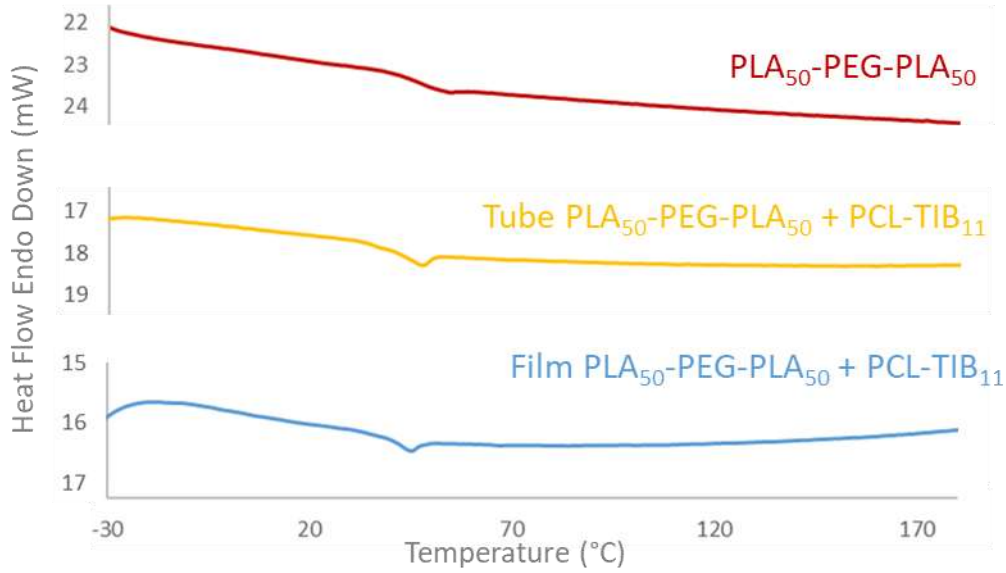

Figure S8. Thermograms of PLA_{50}-PEG-PLA_{50} powder and of the PLA_{50}-PEG-PLA_{50} (90wt%) + $PCL\text{-}TIB_{11}$ (10wt%) blend processed by film evaporation or tube injection.

S9- Impact of the sterilization on the mechanical properties.

A

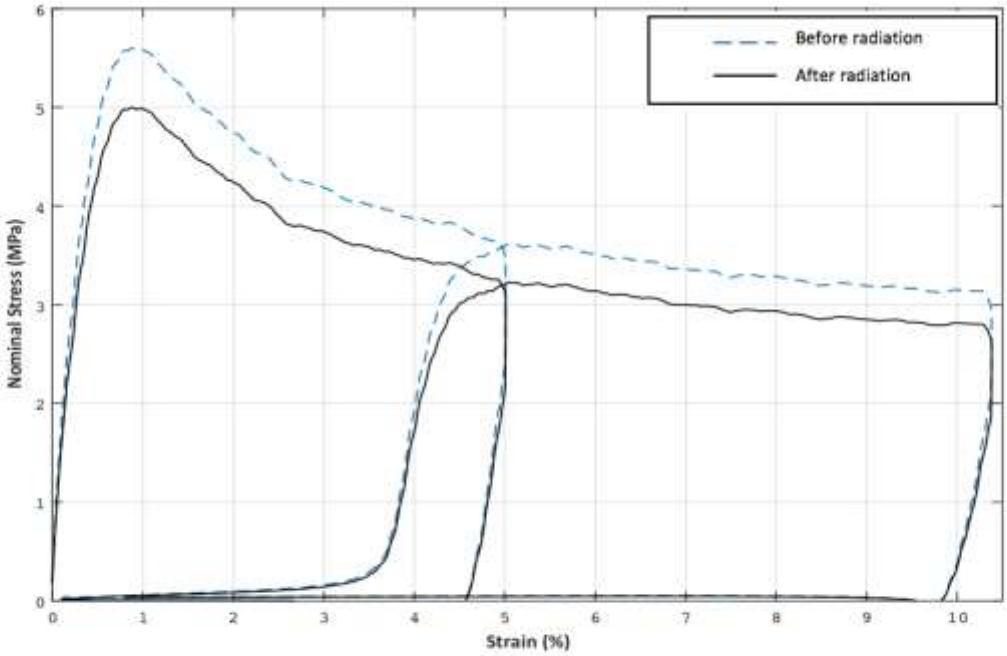

B

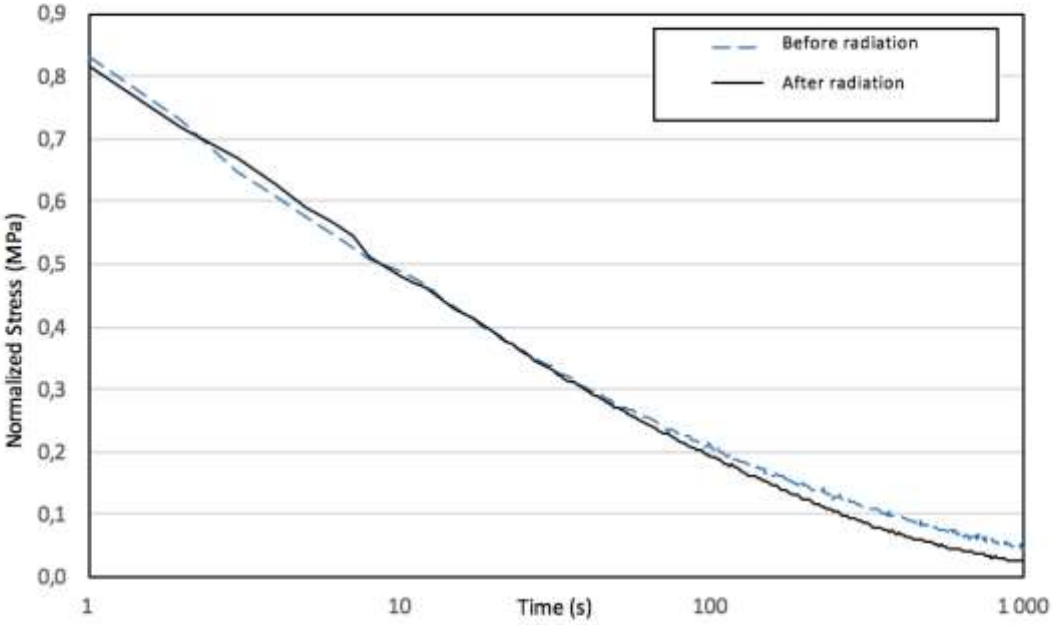

C

	Before γ radiation *(Mean ± SD)*	Before γ radiation *(Mean ± SD)*
E	0,88 ± 0,06	0,44 ± 0,05
$E_{5\%}$	0,23 ± 0,01	0,19 ± 0,01

Figure S9. Mechanical tests before and after gamma radiations (25 kGy).
A. Stress–strain curves for cyclic loading tests
B. Normalized relaxation test during in vivo degradation at 5% strain load.
C. Young's modulus (*E*) and $E_{5\%}$ with and without irradiation